

1 **Evaluation and Modification of ELM Seasonal Deciduous Phenology against**
2 **Observations in a Southern Boreal Peatland Forest**

3 Lin Meng^a, Jiafu Mao^{b,*}, Daniel M. Ricciuto^b, Xiaoying Shi^b, Andrew D. Richardson^{c,d},
4 Paul J. Hanson^b, Jeffrey M. Warren^b, Yuyu Zhou^a, Xuecao Li^c, Li Zhang^f, and Christina Schädel^d

5 *^a Department of Geological and Atmospheric Sciences, Iowa State University, Ames, IA 50011*

6 *^b Environmental Sciences Division and Climate Change Science Institute, Oak Ridge National*
7 *Laboratory, Oak Ridge, TN 37830*

8 *^c School of Informatics, Computing and Cyber Systems, Northern Arizona University, Flagstaff,*
9 *AZ 86011*

10 *^d Center for Ecosystem Science and Society, Northern Arizona University, Flagstaff, AZ 86011*

11 *^e College of Land Science and Technology, China Agricultural University, Beijing 100083,*
12 *China*

13 *^fKey Laboratory of Ecosystem Network Observation and Modeling, Institute of Geographic*
14 *Sciences and Natural Resources Research, Chinese Academy of Sciences, Beijing*

15
16 Corresponding author: Jiafu Mao (maoj@ornl.gov)

17
18 *This manuscript has been authored by UT-Battelle LLC under Contract No. DE-AC05-00OR22725 with the US*
19 *Department of Energy (DOE). The US government retains and the publisher, by accepting the article for*
20 *publication, acknowledges that the US government retains a nonexclusive, paid-up, irrevocable, worldwide license*
21 *to publish or reproduce the published form of this manuscript, or allow others to do so, for US government*
22 *purposes. DOE will provide public access to these results of federally sponsored research in accordance with the*
23 *DOE Public Access Plan (<http://energy.gov/downloads/doe-public-access-plan>).*

24 **Abstract**

25 Phenological transitions determine the timing of changes in land surface properties and the
26 seasonality of exchanges of biosphere-atmosphere energy, water, and carbon. Accurate
27 mechanistic modeling of phenological processes is therefore critical to understand and correctly
28 predict terrestrial ecosystem feedbacks with changing atmospheric and climate conditions.
29 However, the phenological components in the land model of the US Department of Energy's
30 (DOE) Energy Exascale Earth System Model (ELM of E3SM) were previously unable to
31 accurately capture the observed phenological responses to environmental conditions in a well-
32 studied boreal peatland forest. In this research, we introduced new seasonal-deciduous
33 phenology schemes into version 1.0 of ELM and evaluated their performance against the
34 PhenoCam observations at the Spruce and Peatland Responses Under Changing Environments
35 (SPRUCE) experiment in northern Minnesota from 2015 to 2018. We found that phenology
36 simulated by the revised ELM (i.e., earlier spring onsets and stronger warming responses of
37 spring onsets and autumn senescence) was closer to observations than simulations from the
38 original algorithms for both the deciduous conifer (*Larix laricina*) and mixed shrub layers.
39 Moreover, the revised ELM generally produced higher carbon and water fluxes (e.g.,
40 photosynthesis and evapotranspiration) during the growing season and stronger flux responses to
41 warming than the default ELM. A parameter sensitivity analysis further indicated the significant
42 contribution of phenology parameters to uncertainty in key carbon and water cycle variables,
43 underscoring the importance of precise phenology parameterization. This phenological modeling
44 effort demonstrates the potential to enhance the E3SM representation of land-climate interactions
45 at broader spatiotemporal scales, especially under anticipated elevated CO₂ and warming
46 conditions.

47 **Keywords:** Phenology, climate change, PhenoCam, modeling, E3SM, ELM

48 **1 Introduction**

49 Phenological events such as leaf unfolding and flowering are sensitive to variations in weather
50 and climate (Körner and Basler, 2010a). Multiple lines of observations have documented an
51 earlier spring leaf-out, later autumn senescence, and longer growing season in response to
52 warming, especially for terrestrial ecosystems over the northern mid-high latitudes (Körner and
53 Basler, 2010b; Menzel and Fabian, 1999; Piao et al., 2019a; Richardson et al., 2018b).

54 Phenology regulates plant feedbacks to the climate system via the timing changes of land surface
55 biophysical and biogeochemical fluxes and properties (Richardson et al., 2013; Schwartz, 1992;
56 Li et al., 2016). For example, the leaf emergence in spring increases transpiration and latent heat
57 flux but decreases the Bowen ratio (Richardson et al., 2013); earlier spring leaf-out increased
58 annual gross primary production (GPP) by about 10 g C/m² in a temperate deciduous forest
59 (Richardson et al., 2013); and an extension of just 1 day in growing season length may increase
60 the annual GPP of northern terrestrial ecosystems by ~0.5% (Piao et al., 2007; White et al.,
61 2009).

62 Spring onset of seasonal deciduous ecosystems is mainly driven by temperature through
63 underlying physiological processes (Sarvas, 1974). Based on this, the thermal time model was
64 proposed as early as the eighteenth century to predict spring onset as the date when the
65 accumulated growing-degree-day exceeds a threshold (Reaumur, 1735). Later, manipulative
66 experiments revealed that plants need to be exposed to low chilling temperatures to break
67 dormancy before responding to the rising spring temperature (Hannerz et al., 2003; Hänninen
68 et al., 2019; Sarvas, 1972). Chilling models have since been proposed to predict the spring

69 phenology based on a balance between winter chilling requirement and accumulated spring
70 temperature forcing (Cannell and Smith, 1983; Landsberg, 1974; Sarvas, 1972). These models
71 characterize nonlinear responses of spring phenology to temperature (Cesaraccio et al., 2004),
72 and have been widely applied from local to global scales to examine the phenological effects of
73 climate change (Chuine et al., 2016; Meng et al., 2020a; Meng et al., 2020b). More recent
74 models for spring phenology have emerged by integrating the influences of winter chilling,
75 spring thermal forcing, photoperiod (i.e., daylength), and their interactions (Caffarra et al., 2011;
76 Liang, 2019), albeit resulting in greater model complexity and increased model parameters
77 (Chuine and Régnière, 2017; Hänninen et al., 2019).

78 In contrast, autumn senescence such as leaf coloration, reduced functionality of photosynthesis
79 and transpiration, and leaf fall has drawn less attention until recently (Keskitalo et al., 2005;
80 Richardson et al., 2012). Autumn senescence was found to be likely modulated by the decrease
81 in photoperiod and temperature (Fracheboud et al., 2009; Richardson et al., 2018b). Based on the
82 process of cold-degree-day (CDD) accumulation, several leaf senescence models were developed
83 (Dufrêne et al., 2005; Jeong and Medvigy, 2014); the impacts of daylength decrease on the
84 effectiveness of CDD accumulation were later introduced to improve the senescence modeling
85 (Delpierre et al., 2009); and the impact of timing of spring phenology on the autumn senescence
86 process by influencing the requirement of CDD accumulation was also proposed (Keenan and
87 Richardson, 2015). A recent study examining multiple leaf senescence assumptions reported that
88 models considering the interactions between photoperiod and temperature outperformed those
89 solely based on temperature or photoperiod thresholds (Liu et al., 2020), although further
90 mechanistic understanding of leaf senescence is needed.

91 Despite the progress in phenological modeling, the advancement of phenology scheme remains
92 limited in many state-of-the-art land surface models, such as the land model of the US
93 Department of Energy's (DOE) Energy Exascale Earth System Model (ELM of E3SM).
94 Consistent with Community Land Model (CLM) version 4.5, ELM v1.0 includes three distinct
95 phenology types that are represented by separate algorithms: an evergreen type, for which some
96 fraction of annual leaf growth persists for longer than one year; a seasonal-deciduous type with
97 distinct growing and dormant seasons once per year; and a stress-deciduous type with the
98 potential for multiple growing seasons per year (Lawrence et al., 2011). For the seasonal-
99 deciduous model, two processes determine the length of the growing season: spring onset and
100 autumn senescence. Spring onset is merely triggered by the growing-degree-day accumulation of
101 soil temperature, and autumn senescence is set as a constant date at any given location according
102 to a fixed daylength threshold (Oleson, 2013). Although this scheme captures the dominant
103 drivers of seasonal phenology, the ELM phenological simulations were demonstrated to be
104 biased against observational phenology changes and failed to capture interannual variation of
105 phenology (Chen et al., 2016). For example, degraded land model performance was noticed
106 when using the prognostic phenology instead of prescribed, satellite-derived phenology
107 (Lawrence et al., 2011); substantial biases in the intra-annual variation of the fraction of
108 absorbed photosynthetically active radiation were found to be partially caused by phenology
109 errors (Wang et al., 2013). Such uncertainties associated with phenology modeling are not
110 unique for ELM but are typical for most current-generation land surface models. One study
111 systematically evaluated 14 land surface models participating in the North American Carbon
112 Program Site Synthesis and revealed a model bias of about two weeks in the representation of the
113 growing season length and a poor reproduction of the observed inter-annual phenology

114 variability (Richardson et al., 2012). Another more recent multi-land surface model
115 intercomparison study (including CLM 4.5 and 5.0) showed an 18-day delay for the start of the
116 season and a 2-week advancement for the end of the season compared with satellite observations
117 (Peano et al., 2020). Limited efforts, however, have been spent improving the spring onset
118 models using satellite or in situ observations (Chen et al., 2016; Dahlin et al., 2015), and even
119 fewer have been focused on improving the autumn senescence process.

120 The Spruce and Peatland Responses Under Changing Environments (SPRUCE) whole-
121 ecosystem warming experiment in a southern boreal peatland forest provides a unique
122 opportunity to confront the seasonal-deciduous phenology schemes of ELMs at the site level in
123 response to altered environmental conditions. Results from this experiment revealed that
124 warming treatments of up to +9°C caused a linearly advanced spring green-up (1.97 days/°C for
125 *Larix laricina* and 1.99 days/°C for the mixed shrub layer) and delayed autumn green-down
126 (1.34 days/°C for *Larix laricina* and 4.98 days/°C for the mixed shrub layer) (Richardson et al.,
127 2018b). These SPRUCE phenological changes have been monitored automatically every half
128 hour by cameras of the PhenoCam network, which use digital photography with high quality and
129 a standardized approach to track phenology evolutions and facilitate model development
130 (Seyednasrollah et al., 2019). In this study, we first incorporated improved spring onset and
131 autumn senescence models into the ELM as the seasonal-deciduous phenology schemes, in
132 which the spring onset depends on both winter chilling and spring thermal forcing processes
133 whereas the timing of autumn senescence relies on the co-limitation of daylength and
134 temperature. The modified ELM was then calibrated and evaluated against the SPRUCE
135 PhenoCam observations for the period beginning in autumn 2015 through 2018. We also
136 simulated and examined possible phenological feedbacks to major carbon and hydrological

137 variables under various warming and CO₂ levels using the default and updated ELM. The
138 sensitivity of model outputs to the new phenology parameters was further analyzed. The
139 following questions were addressed in this research: (1) How different are the default and
140 phenology-modified ELM versions regarding the prediction of phenology patterns and
141 phenological responses to warming? (2) To what extent are the ELM-simulated exchanges of
142 land-atmosphere carbon and water fluxes affected by the new phenological algorithms? (3) How
143 sensitive are the carbon and water cycle outputs of the updated ELM to uncertainty in major
144 phenology parameters across vegetation types?

145 **2 Materials and Methods**

146 **2.1 Experimental site**

147 The SPRUCE experiment is a large-scale ecological manipulation that evaluates the combined
148 response of a southern boreal peatland to multiple levels of whole-ecosystem warming up to
149 +9°C at both ambient CO₂ (aCO₂) and elevated CO₂ (eCO₂) concentrations (Hanson et al., 2017).
150 This field experiment was designed to investigate how underlying mechanistic processes respond
151 to altered climate conditions, and how the interaction between those processes scale to
152 ecosystem-level responses. SPRUCE consists of large open-top enclosures and is located within
153 a *Picea-Larix—Sphagnum* spp. bog (S1 bog) at the USDA Forest Service Marcell Experimental
154 Forest in northern Minnesota (47° 30.476'N; 93° 27.162'W; 418 m above mean sea level) (Kolka
155 et al., 2011). Situated at the southern extent of the spatially expansive boreal peatland forests,
156 this ecosystem is considered to be near its tipping point with respect to environmental change
157 (Hanson et al., 2020).

158 The bog surface has a hummock/hollow microtopography, where the tops of hummocks are
159 typically 10–30 cm higher than the bottoms of hollows (Shi et al., 2015). There are distinct
160 hydrologic dynamics and vegetation communities between the raised hummock and sunken
161 hollow microtopography characteristic of peatland bogs. The hummock/hollow microtopography
162 allows a greater aerobic rooting profile for shrubs and trees during the wet spring but limits water
163 availability to roots during summer drying periods. At SPRUCE, the primary vegetation types
164 include *Picea mariana* (black spruce) and *Larix laricina* (larch) trees with a mixed deciduous
165 and semi-evergreen Ericaceous shrub layer. The types of mixed shrub layer at SPRUCE mainly
166 include *Rhododendron groenlandicum* (Oeder) Kron and Judd (Labrador tea) and
167 *Chamaedaphne calyculata* (L.) Moench. (leatherleaf). The ground layer vegetation beneath the
168 shrubs within the S1 bog also comprises a bryophyte layer dominated by *Sphagnum* spp. Air and
169 soil warming at five target levels (+0°C, +2.25°C, +4.5°C, +6.75°C, and +9°C) was conducted
170 across different enclosures under aCO₂ or eCO₂ (800 to 900 ppm) conditions. The whole-
171 ecosystem warming began in August 2015, and eCO₂ treatments began in June 2016.

172 **2.2 Phenological and environmental measurements**

173 PhenoCams (i.e., high-resolution digital cameras) record seasonal variation in vegetation
174 “greenness” (i.e., a proxy for vegetation phenology and associated physiological activity) in each
175 SPRUCE enclosure (Richardson et al., 2018a). These cameras were installed at a height of 6 m
176 on the south wall of each enclosure and took images automatically every half hour. A reliable
177 metric of vegetation greenness, green chromatic coordinate (G_{CC}), was derived from each image
178 for three vegetation types: *Picea mariana*, *Larix laricina*, and the mixed shrub layer (Richardson
179 et al., 2007; Sonnentag et al., 2012). G_{CC} increases during spring, reaches its maximum in
180 summer, and decreases during autumn. The estimated transition dates of “greenness rising” in

181 spring and “greenness falling” in autumn were derived when the 3-day smoothed G_{CC} crosses its
182 25% seasonal amplitude threshold for each vegetation type from each enclosure every year
183 (Schädel et al., 2019). In this study, phenological transition dates of *Larix laricina* and the mixed
184 shrub layer from 2015 to 2018 were used to improve the seasonal-deciduous phenological
185 models in the ELM.

186 Related environmental observations from the SPRUCE experiment have been detailed by
187 Hanson et al. (2017). Briefly, the half-hour air temperature was observed at the center of each
188 plot at 0.5, 1, 2, and 4 m above the surface of the peat. Half-hour belowground soil temperatures
189 were measured at three locations (central, middle, and edge) across each plot at the following
190 depths: 0, -0.05, -0.1, -0.2, -0.3, -0.4, -0.5, -1, and -2 m, where 0 m is the peatland hollow
191 height (low points in an undulating surface). In this study, we used spatially averaged soil
192 temperatures simulated at -0.05 m (which is the third soil layer in the ELM) and the observed 2
193 m air temperature within each enclosure to stimulate phenology in the default and revised ELM
194 as described in the next section.

195 **2.3 Default phenological schemes in the ELM**

196 The default seasonal-deciduous phenology schemes in the ELM, which include spring onset and
197 autumn senescence models, were adapted from the phenology algorithms designed for temperate
198 deciduous broadleaf forest (Thornton et al., 2002; White et al., 1997). The spring onset occurs
199 when the growing-degree-day accumulation (GDD_{sum}) of the third-layer soil temperature ($T_{s,3}$,
200 in kelvin) initiated at the winter solstice exceeds a threshold GDD_{sum_crit} . GDD_{sum_crit} is
201 determined by the annual average 2 m air temperature in the preceding year ($T_{2m,ann_{avg}}$, in
202 kelvin).

203
$$GDD_{sum} = \sum(T_{s,3} - TKFRZ) , \quad (1)$$

204
$$GDD_{sum_crit} = \exp(4.8 + 0.13 \times (T_{2m,ann_{avg}} - TKFRZ)) , \quad (2)$$

205 where $TKFRZ$ is the freezing point of water (273.15 K).

206 Because plants across regions require different degrees of warming (i.e., GDD_{sum_crit} here) to
207 initiate growth, Eq. (2) of GDD_{sum_crit} was calculated as a function of mean annual temperature
208 in the preceding year to accommodate spatial phenology simulation at a broader scale (White
209 et al., 1997). However, this calculation may cause incorrect responses of spring phenology to
210 warming (see Section 4).

211 The autumn senescence is simulated to occur when the daylength is shorter than 39,300 s (about
212 10.9 h). Because daylength is calculated as a function of latitude and day of the year (Forsythe et
213 al., 1995), the default autumn senescence date is temporally invariant for any given location.

214 **2.4 Revised phenological models**

215 Different spring and autumn phenology models in previous studies have been widely
216 intercompared and evaluated (Cannell and Smith, 1983; Delpierre et al., 2009; Landsberg, 1974;
217 Migliavacca et al., 2008; Murray et al., 1989; Sarvas, 1972). For application to the ELM, the
218 alternating model for spring onset (Murray et al., 1989) and the CDD model proposed by
219 Delpierre et al. (2009) (hereafter termed “DM”) for autumn senescence were selected because of
220 their mechanistic assumption, performance, and simplicity.

221 For the alternating model, the spring onset is simulated through winter chilling and spring
222 thermal forcing processes. The state of chilling (S_c) or forcing (S_f) is the time integral from t_0

223 (i.e., winter solstice here) of the rate of chilling (R_c) or forcing (R_f). R_f is the relative daily
 224 temperature above the base temperature (T_{base}), and R_c is 1 if the daily mean temperature $T(t)$ is
 225 below T_{base} and is otherwise 0.

$$226 \quad R_f(t) = \begin{cases} T(t) - T_{base} & T(t) > T_{base} \\ 0 & T(t) \leq T_{base} \end{cases}, \quad (3)$$

$$227 \quad S_f(t) = \sum_{t_0} R_f(T(t)), \quad (4)$$

$$228 \quad R_c(t) = \begin{cases} 1 & T(t) < T_{base} \\ 0 & T(t) \geq T_{base} \end{cases}, \quad (5)$$

$$229 \quad S_c(t) = \sum_{t_0} R_c(T(t)). \quad (6)$$

230 Spring leaf-out occurs when

$$231 \quad S_f(t) \geq a + b * \exp(c * S_c(t)), \quad (7)$$

232 where $c < 0$. a , b , c , and T_{base} are parameters to be calibrated.

233 For the DM, the progress of the leaf senescence is represented through a CDD sum and a
 234 photoperiod decrease process. The coloring state (S_{sen}) is the time integral at the rate of R_{sen}
 235 starting when daily daylength $P(t)$ is shorter than a photoperiod threshold P_{start} , which varies
 236 with latitudes. R_{sen} is a function of temperature and photoperiod and only accumulates when the
 237 daily mean temperature $T(t)$ is below the base temperature T_b . The function of R_{sen} means a
 238 stronger CDD sum effect under short photoperiod conditions relative to P_{start} .

$$239 \quad \text{If } P(t) < P_{start} \quad \text{if } \begin{cases} T(t) < T_b \\ T(t) > T_b \end{cases} \quad R_{sen}(t) = \begin{cases} (T_b - T(t)) * (1 - \frac{P(t)}{P_{start}}) \\ R_{sen}(t) = 0 \end{cases}, \quad (8)$$

240
$$S_{sen}(t) = \sum R_{sen}(t) \cdot \tag{9}$$

241 Autumn senescence is simulated to occur when $S_{sen}(t) \geq Y_{crit}$. Y_{crit} , P_{start} , and T_b are
242 parameters to be calibrated.

243 The spring alternating model and autumn DM were first calibrated using the PhenoCam
244 observations from 2016 to 2017 and 2015 to 2017, respectively, across all enclosures and were
245 then evaluated using the PhenoCam data during 2018 (Table S1, S2). The model calibration was
246 performed based on the minimum root mean square error (RMSE) between simulated phenology
247 and observations (20 enclosure-years of data for spring onset and 30 enclosure-years of data for
248 autumn senescence). Independent model calibration and evaluation were separately conducted
249 for *Larix laricina* trees and the mixed shrub layer.

250 **2.5 Phenology comparison between PhenoCam and the ELM**

251 Because the phenological transition dates from PhenoCam and the ELM are defined differently,
252 we adjusted the PhenoCam observations to make them directly comparable with the ELM
253 phenology outputs. In the ELM, the spring onset is the timing when leaf area index (LAI) starts
254 to increase from 0, and the autumn senescence is the timing when LAI begins to decrease from
255 its maximum value. Within a fixed 30-day period after spring onset, the ELM LAI increases to
256 its maximum value and stays the same until the autumn senescence occurs; within a fixed 15-day
257 period after the start of autumn senescence, the ELM LAI then decreases to 0. In contrast, the
258 spring green-up and autumn green-down dates from PhenoCam represent the timings
259 corresponding to 25% seasonal amplitude of greenness. Therefore, we adjusted the PhenoCam
260 observations by subtracting 7.5 days ($25\% \times 30$ days) from spring green-up dates and by
261 subtracting 11.25 days ($(1\% - 25\%) \times 15$ days) from autumn green-down dates, and we performed

262 the ELM evaluation and calibration processes using the updated observational timings. This
263 adjustment is valid based on abundant previous studies showing that the temporal development
264 of plant LAI was synchronous with PhenoCam G_{CC} , especially for deciduous forests, and they
265 both represent canopy development (Liu et al., 2015; Cremonese et al., 2017; Peichl et al., 2015).

266 **2.6 ELM-SPRUCE**

267 In this study, we used the SPRUCE version of the ELM, which was developed mainly for the
268 ELM improvements and simulations at SPRUCE. New functions in this ELM version include
269 revised hydrological parameters, representation of hummock and hollow microtopography and
270 lateral flows, the inclusion of more mechanistic CH_4 processes, and *Sphagnum* dynamics
271 (Hanson et al., 2020; Ricciuto et al., 2020; Shi et al., 2015). However, until this study, the
272 representation of seasonal deciduous phenology was unchanged from CLM4.5 (Oleson, 2013).
273 For the ELM, one land grid comprises five primary units—glacier, lake, wetland, urban, and
274 vegetation—at different fractional coverages. Within each grid cell, the vegetated portion is
275 further divided into patches of plant functional types (PFTs), with each possessing unique
276 vegetation properties but sharing the same environmental forcings and soil conditions (Oleson,
277 2013). Thus, the ELM produces both grid- and PFT-level outputs, with the latter having
278 connected carbon, water, and energy summaries across different PFTs. At SPRUCE, four PFTs
279 coexisted within one ELM grid cell (i.e., enclosure here)—boreal needleleaf evergreen tree,
280 boreal needleleaf deciduous tree, boreal broadleaf shrub, and moss (*Sphagnum*). We only
281 focused on two PFTs that have seasonal-deciduous characteristics in the ELM: *Larix laricina*
282 trees (boreal needleleaf deciduous tree) and mixed shrub layer (boreal broadleaf shrub). Also, we
283 examined the phenology-relevant changes at the PFT and grid-cell levels for each enclosure from
284 the original and improved ELMs.

285 We performed the ELM simulations using the default and revised phenological algorithms
286 (hereafter referred to as “ELM_Default” and “ELM_New,” respectively). ELM_New includes
287 the alternating model for spring onset and DM for autumn senescence introduced in Section 2.4.
288 We conducted ELM simulations for three phases: accelerated decomposition spin-up, final spin-
289 up, and transient. Each spin-up generated an equilibrium state to estimate the relative content of
290 carbon, nitrogen, and phosphorus in different vegetation and soil pools. For the first part of the
291 transient phase, we conducted a run from 1850 to 2010 driven by the SPRUCE-observed cycling
292 of meteorology variables for 2011 to 2018 and the historical changes of other environmental
293 forcings at the ambient enclosures (e.g., atmospheric CO₂ concentrations, nitrogen deposition).
294 Then, for the 2011 to 2018 period, we ran 10 ELM simulations (2 CO₂ concentrations × 5
295 warming levels) using the SPRUCE-manipulated temperatures and CO₂ concentrations that were
296 observed in the enclosures; other forcings were kept the same with transient for each ELM
297 version. We systematically intercompared the PFT-level model outputs from ELM_Default and
298 ELM_New in terms of spring onset, autumn senescence, and major carbon and water fluxes (i.e.,
299 total LAI (TLAI), GPP, canopy transpiration (QVEGT), and canopy evaporation (QVEGE))
300 across different warming and CO₂ levels during 2016 to 2018 at monthly, seasonal, and annual
301 scales. We also examined main carbon and water variables at the grid-cell level for the hummock
302 and hollow surfaces.

303 **2.7 Sensitivity analysis**

304 Quantifying parameter uncertainty could reveal the impact of certain parameters on key carbon
305 and water variables. We thus used a global sensitivity analysis (GSA) to examine the parameter
306 uncertainty in ELM_New, including phenology- and non-phenology-related parameters, on
307 carbon and water variables. GSA, also called “variance-based decomposition”, attributes

308 variations in predictions to specific model parameters and their interactions given ranges of
309 possible values for the parameters. Following Sargsyan et al. (2014) and Ricciuto et al. (2018),
310 we used Polynomial Chaos surrogate models via a Bayesian compressive sensing approach to
311 conducting the GSA. A surrogate model is a functional representation of a model quantity of
312 interest (QoI) that is constructed from an ensemble of simulations from ELM_New and allows
313 for further exploration of responses over the complex multi-dimensional parameter space. In this
314 case, we performed a total of 10 QoIs representing 5 model output variables averaged over the
315 2011 to 2018 period for each of the two deciduous PFTs: GPP, net primary productivity (NPP),
316 QVEGT, total vegetation carbon (TOTVEGC), and TLAI. For this GSA, we only considered the
317 ambient case with no experimental temperature or CO₂ treatments. Bayesian compressive
318 sensing allows the construction of surrogates using a limited number of simulations, leading to
319 computational cost reduction in studies that otherwise require an infeasible number of ELM
320 simulations, such as GSA or model tuning. We employed the Uncertainty Quantification Toolkit
321 for the Bayesian compressive sensing surrogate construction and GSA (Debusschere et al.,
322 2015), available at <https://github.com/sandialabs/UQTk>.

323 We used 2,000 ELM_New simulations to construct the surrogate model and conducted the GSA.
324 Although we only analyzed QoIs from the deciduous PFTs, we also varied the *Sphagnum* and
325 *Picea* PFT parameters to assess potential interactions with these types. Therefore, 44 model
326 parameters (some of them PFT-specific), including plant trait and soil parameters detailed in Shi
327 et al. (2020) and 7 new phenology parameters, were varied as uniform random variables over
328 their respective reasonable ranges (Table S3). Main effect indices were calculated for each
329 parameter, accounting for individual fractional contributions toward the overall QoI variance.
330 These sensitivity indices do not provide information about whether a parameter has a positive or

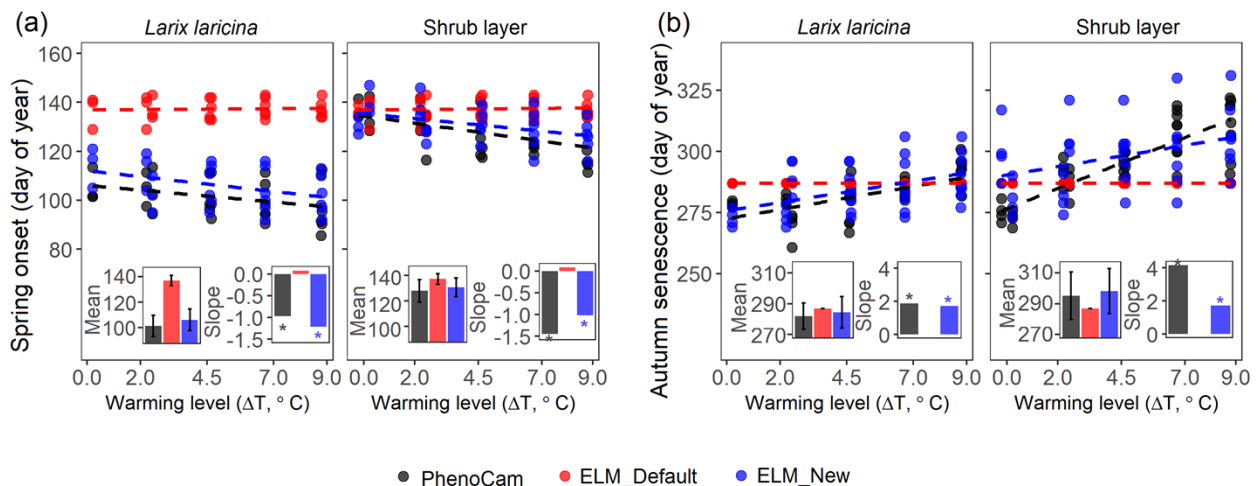
331 negative effect on a QoI. Therefore, using the same 2,000 model samples, we also derived the
332 linear correlation coefficient between each parameter and each QoI to further understand the
333 impacts of individual parameters.

334 **3 Results**

335 **3.1 Phenological evaluations and improvements**

336 Compared with ELM_Default, ELM_New—which includes phenology parameters calibrated
337 against the PhenoCam observations—showed substantial improvement in predicting phenology
338 and the temperature responses of phenology for both *Larix laricina* and the shrub layer. For the
339 simulated spring onset, ELM_New showed a higher correlation (r) with PhenoCam observations
340 (e.g., 0.34 of *Larix laricina* and 0.50 of the shrub layer) compared with that from ELM_Default
341 (corresponding to 0.18 and 0.41) based on the independent model evaluation in 2018 (Table S2).
342 The RMSE of spring onset between ELM_Default simulations and PhenoCam observations for
343 *Larix laricina* was 26 days, which decreased to 8 days when using ELM_New (Table S2).
344 However, for the shrub layer, the RMSE between simulated and observed spring onset was lower
345 for ELM_Default (3.4 days) than for ELM_New (7.4 days), likely because of the unusual
346 weather conditions in 2018. The spring frost in early April 2018 and the following abrupt
347 increase in temperature triggered spring onset to occur later than normal but quickly across all
348 enclosures (standard deviation of spring onset across all enclosures was 3.8 days in 2018
349 compared with 6.8 days in 2016 and 2017, Fig. S1). This appears to be an abnormal phenological
350 response to various warming levels across enclosures, coincidentally better simulated by
351 ELM_Default than ELM_New.

352 For the simulated spring onset during 2016 to 2018, ELM_Default (day of the year: 137 ± 4) was
 353 biased late for both *Larix laricina* (36 days) and the shrub layer (9 days) (Fig. 1a). In contrast,
 354 the spring onset simulated by ELM_New (day of the year: 106 ± 9 for *Larix laricina* and 130 ± 7
 355 for the shrub layer) was only 5 and 2 days later than the PhenoCam observations (left subfigures
 356 in Fig. 1a). In terms of the temperature responses of spring onset, ELM_New (-1.2 days/ $^{\circ}\text{C}$ for
 357 *Larix laricina* and -1.0 days/ $^{\circ}\text{C}$ for the shrub, $P < 0.1$) well captured the observed advancement
 358 of spring onset responding to warming (-1.0 days/ $^{\circ}\text{C}$ and -1.5 days/ $^{\circ}\text{C}$, $P < 0.1$), whereas
 359 ELM_Default failed to capture phenology trends associated with warming ($P > 0.1$) (right
 360 subfigures in Fig. 1a), consistent with previous studies (Chen et al., 2016).



361 **Fig. 1. Observed and simulated responses of spring onset (a) and autumn senescence (b) to**
 362 **warming at SPRUCE.** Linear regression lines are shown as dashed lines. The mean phenology
 363 across all warming and CO₂ levels and slopes of phenology against warming levels are shown in
 364 the subfigures. The error bars in the subfigures represent the standard deviations of phenology
 365 across all warming levels. Significance $P < 0.1$ from two-tailed Student's t test. Spring onset was
 366 during 2016 to 2018, and autumn senescence was during 2015 to 2018.

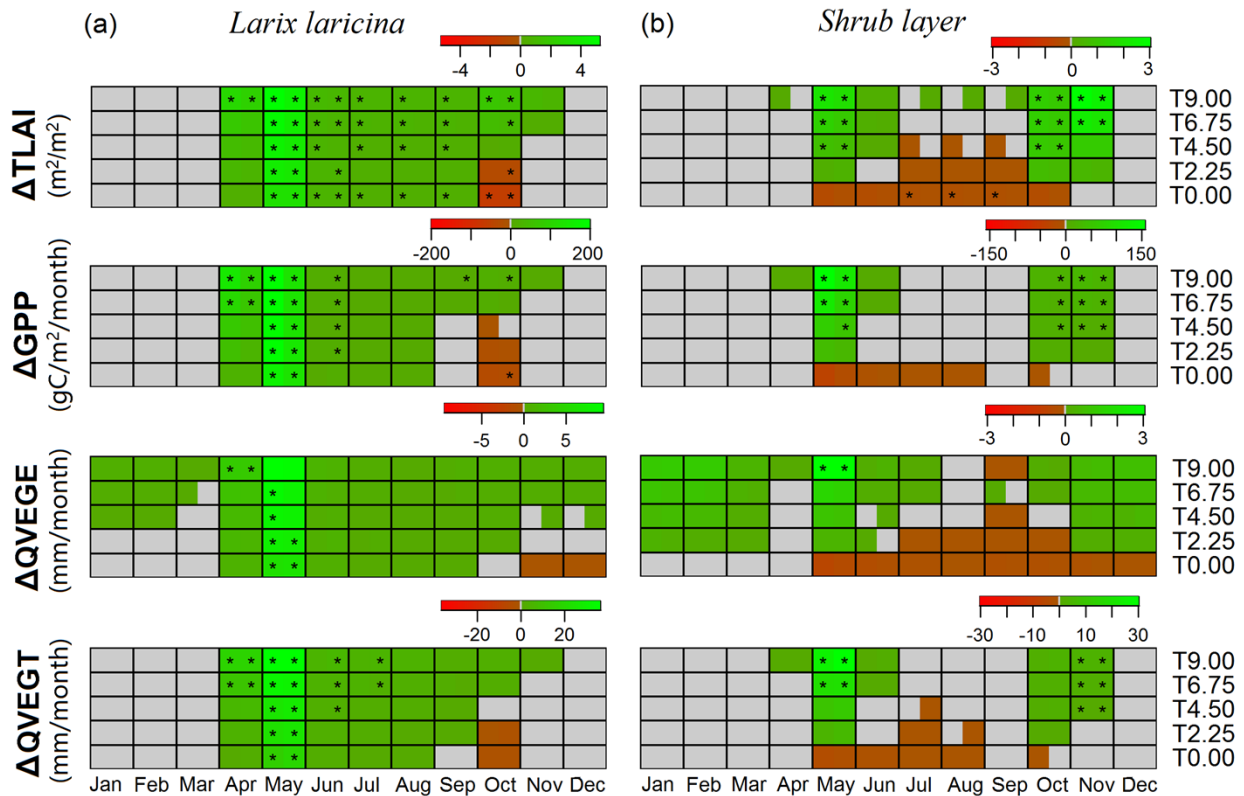
368
 369 ELM_Default simulated the same autumn senescence across the two vegetation types (day of
 370 year: 287 ± 0), with 6 days later for *Larix laricina* but 8 days earlier for the shrub layer than the
 371 PhenoCam, and produced no phenological responses to warming during 2015 to 2018 (Fig. 1b).
 372 In contrast, ELM_New (day of year: 284 ± 10 for *Larix laricina* and 298 ± 15 for the shrub

373 layer) simulated autumn senescence only 3 days later than that of PhenoCam (day of year: $281 \pm$
374 8 and 295 ± 15) for both *Larix laricina* and the shrub layer. More notably, ELM_New (1.72
375 days/°C for *Larix laricina* and 1.74 days/°C for the shrub layer, $P < 0.1$) captured comparable
376 delay trends under warming with the PhenoCam (1.88 days/°C and 4.16 days/°C, $P < 0.1$), albeit
377 with underestimated magnitude for the shrub layer.

378 **3.2 Phenological effects on PFT-level carbon and water fluxes**

379 Mean seasonal cycles of carbon and water fluxes from both ELM_Default and ELM_New were
380 similar in general—TLAI, GPP, and QVEGT peaked during summer, whereas canopy
381 evaporation (QVEGE) showed two peaks in May and October (Figs. S2, S3). Both versions also
382 simulated similar responses of carbon and water fluxes to temperatures and CO₂—TLAI, GPP,
383 QVEGE, and QVEGT showed higher values at warmer levels, and all but QVEGT showed
384 higher values at eCO₂ than aCO₂ conditions (Fig. S2). However, for *Larix laricina*, ELM_New
385 simulated significantly higher annual TLAI, GPP, QVEGE, and QVEGT than those of
386 ELM_Default ($P < 0.1$, Fig. S4a). Such high fluxes occurred mainly during the growing season
387 (i.e., positive difference, represented by green, Fig. 2a), indicating an increase in ecosystem
388 productivity and water fluxes through the extended period of active carbon uptake induced by the
389 early onset of spring. The magnitude of differences between ELM_Default and ELM_New in
390 TLAI (Δ TLAI), GPP (Δ GPP), QVEGE (Δ QVEGE), and QVEGT (Δ QVEGT) was the largest
391 during spring transition periods, especially at higher warming levels and eCO₂ conditions (Fig.
392 2a). Δ TLAI was significant during most of the growing season, whereas Δ GPP, Δ QVEGE, and
393 Δ QVEGT were evident only during spring transition periods and a few other months at the
394 highest warming levels ($P < 0.1$, Fig. 2a). The largest phenology scheme-induced differences
395 occurred in May at the 9°C warming and eCO₂ conditions—5.27 for Δ TLAI ($P < 0.1$), 200.7

396 gC/m²/month for Δ GPP ($P < 0.1$), 9.5 mm/month for Δ QVEGE, and 35.5 mm/month for
 397 Δ QVEGT ($P < 0.1$) (Fig. 2a). ELM_New simulated lower TLAI, GPP, and QVEGT in October
 398 and lower QVEGE in November and December than those of ELM_Default at relatively low
 399 warming levels (i.e., negative difference, represented by brown, Figs. 2a and S4a), indicating an
 400 early reduction of land flux caused by earlier autumn senescence from ELM_New.



401 **Fig. 2. Multi-year mean differences in simulated monthly TLAI, GPP, QVEGE, and**
 402 **QVEGT between ELM_New and ELM_Default for *Larix laricina* (a) and the shrub layer**
 403 **(b) during 2016 to 2018.** Green represents higher values by ELM_New, brown represents lower
 404 values by ELM_New, and gray represents no differences between ELM_New and ELM_Default.
 405 Two pixels are in each grid; left and right pixels represent values under eCO₂ and aCO₂
 406 conditions, respectively. Stars indicate significant differences between ELM_New and
 407 ELM_Default based on a two-tailed Student's *t* test ($P < 0.1$).
 408

409
 410 For the shrub layer, the higher TLAI, GPP, and QVEGT simulated by ELM_New occurred only
 411 during the spring and autumn transition periods, and the higher QVEGE occurred during the
 412 transition periods and non-growing season under 2.25°C or higher warming levels (Fig. 2b). This

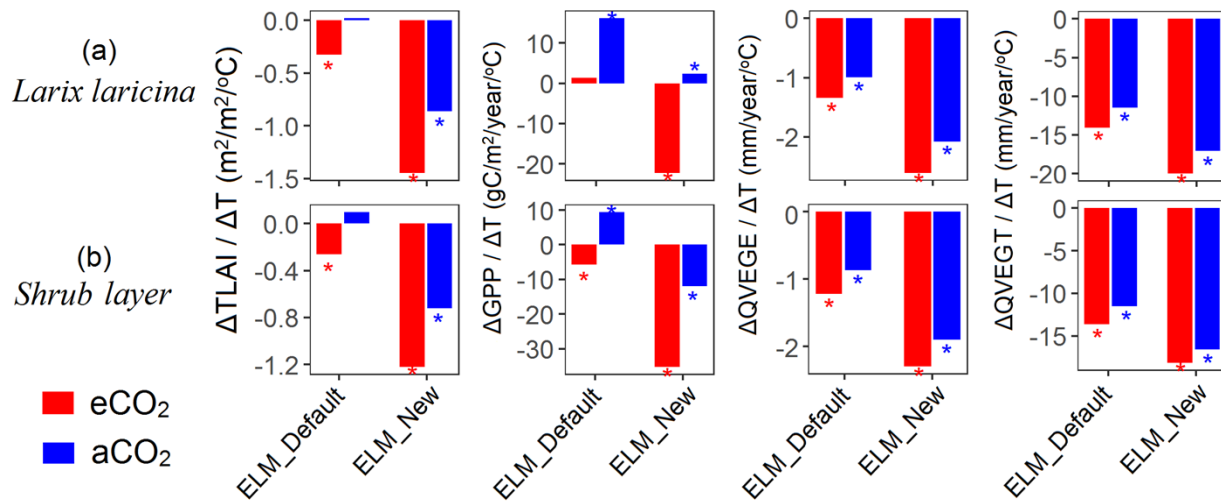
413 indicates the extended growing season of the shrub layer only extended the length of the active
414 land flux period but did not change the magnitude of growing-season land flux, which is
415 different from that of *Larix laricina*. In contrast, within the 0°C warming enclosures, the above
416 variables were lower from ELM_New during the growing season. This corresponds to the
417 phenological changes in Fig. 1 (see Section 4). Such increased TLAI, GPP, QVEGE, and
418 QVEGT by ELM_New were more significant at the warmer enclosures ($P < 0.1$). The largest
419 Δ TLAI (3.1) occurred in November, whereas the largest Δ GPP (157.2 gC/m²/month), Δ QVEGE
420 (3.1 mm/month), and Δ QVEGT (30.3 mm/month) occurred in May at the 9°C warming level (P
421 < 0.1). The magnitudes of change in TLAI, GPP, QVEGE, and QVEGT were smaller for the
422 shrub layer than those for *Larix laricina*.

423 ELM_New also simulated closer seasonality of TLAI and GPP to the seasonality of G_{CC}
424 compared with ELM_Default (normalized value, Figs. S5, S6). For example, in spring 2017, the
425 timing of the increase in TLAI and GPP for *Larix laricina* simulated by ELM_New was
426 concurrent with the timing of the increase in G_{CC} , whereas that by ELM_Default was much later
427 (Fig. S5).

428 **3.3 Temperature responses of carbon and water fluxes at the PFT level**

429 The enhanced phenological responses to warming strengthened the responses of carbon and
430 water fluxes to warming simulated by ELM_New. Although both model versions generally
431 produced stronger responses under the eCO₂ than the aCO₂, ELM_New simulated overall
432 stronger responses of annual TLAI, GPP, QVEGE, and QVEGT to warming than those by
433 ELM_Default (Fig. 3). For *Larix laricina* at the eCO₂, the temperature responses of TLAI and
434 GPP by ELM_New were 4.5 and 17 times stronger, respectively, than by ELM_Default, though

435 the GPP response by ELM_New at the aCO₂ was weaker (Fig. 3a). The responses of QVEGE
 436 and QVEGT to warming were strengthened approximately 2 and 1.5 times, respectively, by
 437 ELM_New compared with ELM_Default. For the shrub layer, the temperature responses of
 438 carbon and water fluxes showed similar patterns to those of *Larix laricina* but with weaker
 439 magnitudes except for GPP (Fig. 3b). Such enhanced responses of TLAI and GPP to warming by
 440 ELM_New are also shown in Figs. S5 and S6; the time series of TLAI and GPP by ELM_New
 441 were more dispersed across warming levels during the spring and autumn transition periods,
 442 which better matched G_{CC} .



443

444 **Fig. 3. Temperature responses of annual TLAI, GPP, QVEGE, and QVEGT simulated by**
 445 **ELM_Default and ELM_New for *Larix laricina* (a) and the shrub layer (b).** We used annual
 446 average TLAI (m²/m²) and GPP (gC/m²/year), and annual sum QVEGE (mm/year) and QVEGT
 447 (mm/year). The temperature responses were calculated as the slope of the linear regression
 448 between annual TLAI, GPP, QVEGE, and QVEGT and warming levels. Stars indicate
 449 significance from linear regression ($P < 0.1$). Results for each season are shown in Figs. S7
 450 and S8.

451

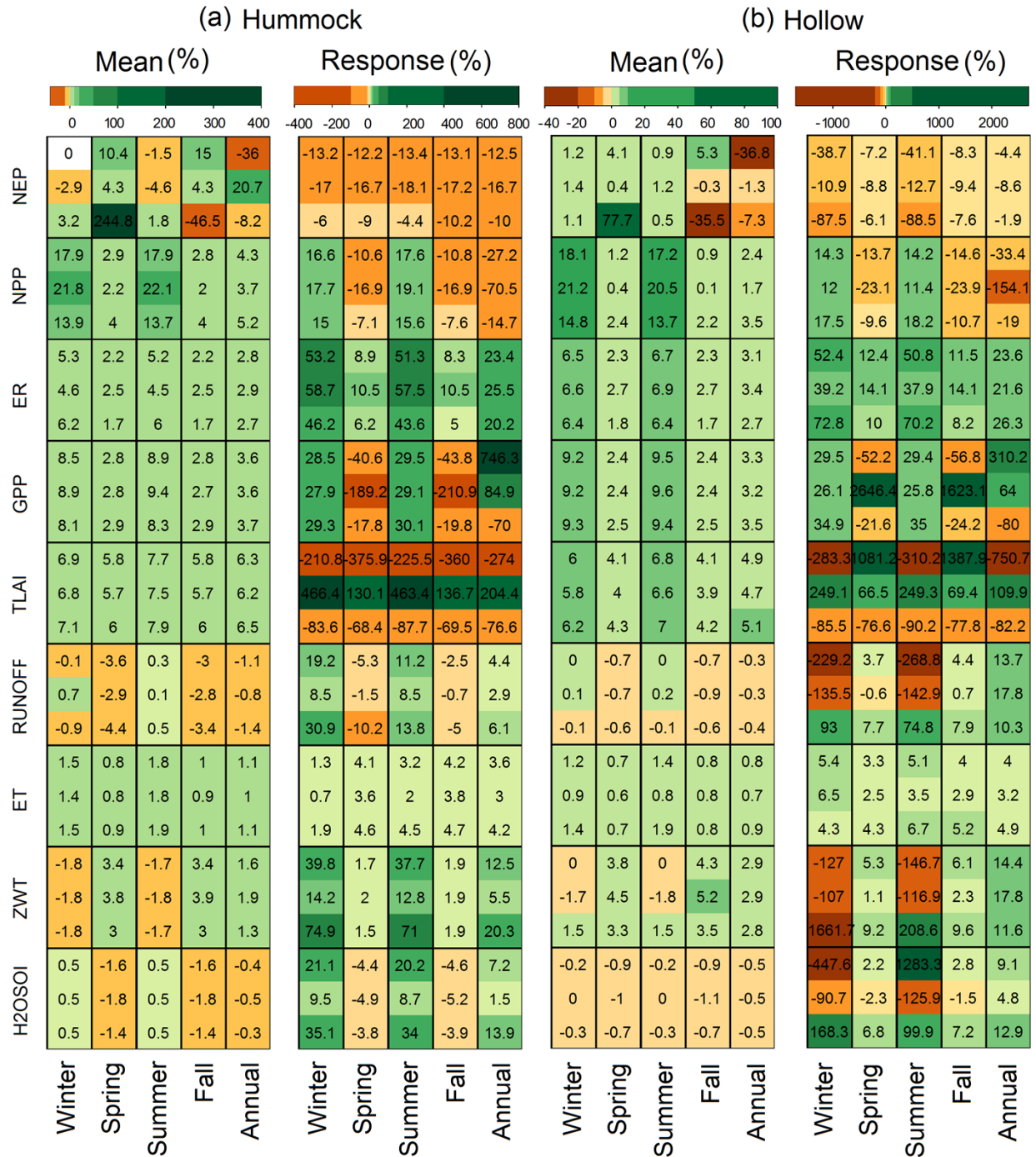
452 The temperature responses of the selected land surface variables displayed distinct patterns
 453 across seasons (Figs. S7, S8, no value in winter). During the spring and autumn, ELM_Default
 454 simulated small responses of TLAI and GPP to warming, but ELM_New simulated prominent

455 responses for both *Larix laricina* (Fig. S7) and the shrub layer (Fig. S8). The differences in the
456 annual response of QVEGE and QVEGT simulated by ELM_Default and ELM_New (Fig. 3)
457 primarily came from spring, where, for example, ELM_New (-0.93 mm/season/ $^{\circ}$ C) simulated
458 383% higher QVEGE than that of ELM_Default (-0.24 mm/season/ $^{\circ}$ C) at eCO₂ for *Larix*
459 *laricina* (Fig. S7). In summer, the temperature responses of the selected land surface variables
460 were very similar.

461 The magnitudes of Δ TLAI and Δ GPP between ELM_New and ELM_Default were well
462 correlated with the difference magnitudes in phenology (Fig. S9). The Δ TLAI and Δ GPP in May
463 were positively correlated with the differences in spring onset between ELM_New and
464 ELM_Default for the shrub layer ($P < 0.01$, Fig. S9b). However, for *Larix laricina*, only Δ TLAI
465 at the eCO₂ showed a positive correlation ($P = 0.02$, Fig. S9a). Likewise, the difference
466 magnitude in autumn senescence was positively correlated with the magnitude of Δ TLAI and
467 Δ GPP in October (Fig. S9c, d). This corresponds to Figs. 1 and 2; the earlier autumn senescence
468 at low warming levels by ELM_New led to reduced magnitudes in TLAI and GPP in autumn.
469 However, the later senescence at high warming levels by ELM_New caused increased
470 magnitudes in TLAI, GPP, QVEGE, and QVEGT. The responses of TLAI and GPP to changes
471 in phenology were more prominent in eCO₂ than in aCO₂ and for *Larix laricina* than the shrub
472 layer (higher slopes). Interestingly, for the shrub layer, the responses of TLAI and GPP to
473 changes in spring onset were much stronger than their responses to changes in autumn
474 senescence, but opposite for *Larix laricina*. The enhanced temperature responses of spring onset
475 and autumn senescence (Fig. 1) also contributed to the larger temperature responses in TLAI,
476 GPP, QVEGE, and QVEGT by ELM_New (Fig. 3).

477 3.4 Phenological feedbacks to carbon and water fluxes at the grid-cell level

478 Grid average carbon and water fluxes showed distinct changes simulated by ELM_Default and
479 ELM_New (Fig. 4). Such grid-cell-level patterns reflect the combined responses of all PFTs—
480 *Larix laricina* trees (boreal needleleaf deciduous tree), mixed shrub layer (boreal broadleaf
481 shrub), *Picea mariana* (boreal needleleaf evergreen tree), and *Sphagnum* (moss)—among which
482 the phenology schemes of the former two were revised and the latter two remained the same in
483 ELM_New compared to ELM_Default. ELM_New simulated higher magnitudes of seasonal and
484 annual grid-cell NPP, ecosystem respiration (ER), GPP, TLAI, and ecosystem evapotranspiration
485 (ET) than ELM_Default for both hummock and hollow (Fig. 4). The ELM_New net ecosystem
486 production (NEP) was also higher than that of ELM_Default during spring (e.g., 245% higher at
487 aCO₂) and autumn but lower during winter and summer (e.g., 47% lower at aCO₂) for hummock.
488 Runoff, water table depth (ZWT), and volumetric soil water (H2OSOI) showed various degrees
489 of decrease simulated by ELM_New for both hummock and hollow, and the magnitude of
490 decrease was larger for hummock than hollow. The relative changes in ZWT and H2OSOI were
491 opposite—ELM_New simulated higher H2OSOI but lower ZWT in winter and summer, and
492 reversed patterns for spring and autumn.



493
 494 **Fig. 4. Relative changes in mean and temperature responses in carbon and water fluxes of**
 495 **hummock (a) and hollow (b) simulated by ELM_New compared with ELM_Default.**
 496 Relative changes = $(ELM_New - ELM_Default) / ELM_Default \times 100\%$. Mean carbon and
 497 water fluxes represent the average values across all warming levels, and temperature responses
 498 represent the changes in carbon and water fluxes per degree warming. Green represents a higher
 499 value or stronger response simulated by ELM_New, and brown represents lower values or
 500 weaker response by ELM_New. For each variable, each of the three rows within each grid

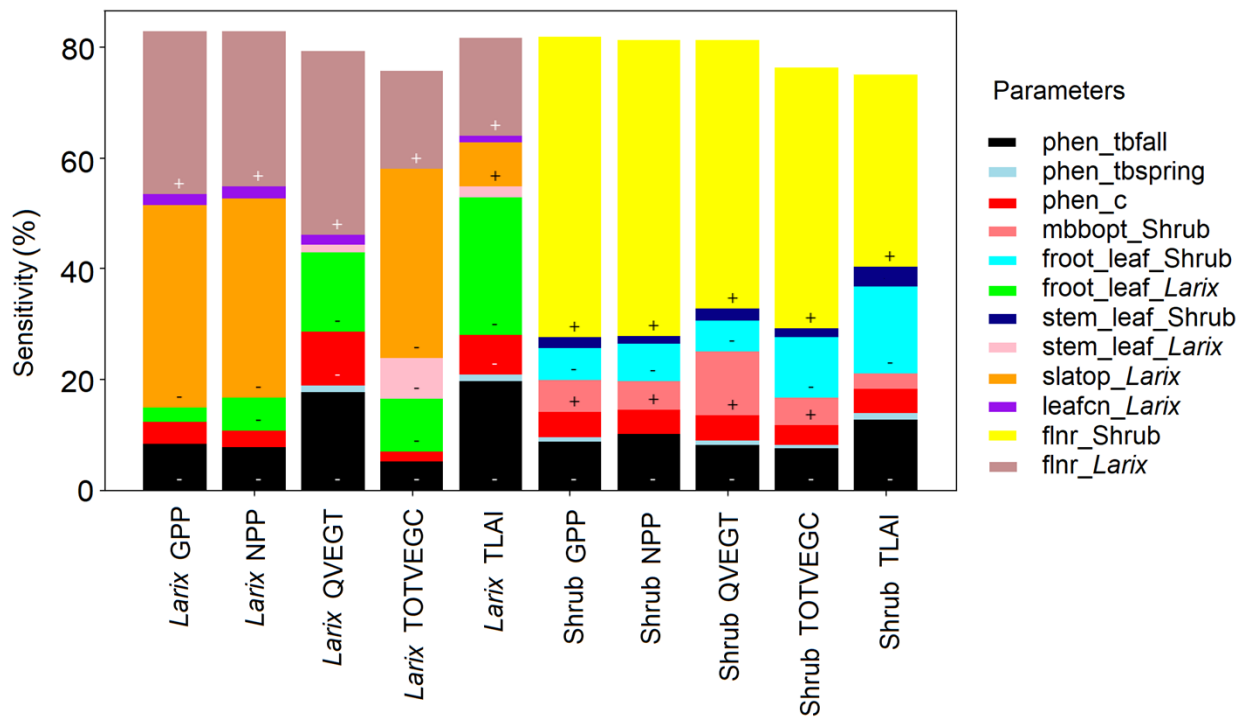
501 represents the mean under eCO₂ and aCO₂ condition, eCO₂ condition, and aCO₂ condition across
502 all warming levels during 2016 to 2018.

503
504 In terms of the responses of carbon and water fluxes to warming (i.e., changes in carbon and
505 water fluxes per degree warming), TLAI showed the largest changes for both hummock and
506 hollow compared with other variables, indicating evident impacts of phenology on TLAI at the
507 grid-cell level. The temperature response of NEP decreased, whereas those for ER, runoff, ET,
508 and ZWT generally increased for the hummock and hollow simulated by ELM_New. The
509 temperature responses of NPP and GPP showed similar seasonal changes—the responses were
510 stronger in winter and summer but weaker in spring and autumn. The seasonal changes in runoff,
511 ZWT, and H2OSOI were opposite for hummock and hollow, with larger changing magnitudes
512 for hollow. These findings indicate significant interactions among individual PFTs within a grid,
513 as well as prominent phenological impacts of the deciduous PFTs on carbon and water fluxes at
514 the grid-cell level.
515

516 **3.5 Sensitivity analysis of ELM_New parameters**

517 To assess the impact of phenology uncertainty on ELM simulations of carbon and water cycling,
518 we conducted a GSA of 10 model outputs to 44 parameters in ELM_New (Fig. 5). Out of the 44
519 total parameters (Table S3), only 12 parameters, including 3 phenology parameters, were
520 responsible for more than 1% of the uncertainty (i.e., sensitivity > 1%, shown in Fig. 5) for at
521 least one of the examined carbon and water variables. For *Larix laricina*, the responses were
522 dominated by the *Larix* fraction of leaf nitrogen in RuBisCO (*flnr_Larix*), the *Larix*-specific leaf
523 area at the top of the canopy (*slatop_Larix*), the *Larix* fine root to leaf allocation ratio
524 (*froot_leaf_Larix*), the *phen_tbfall* (*Tbase* in equation 3), and *phen_c* (*c* in equation 7)
525 parameters. The leaf and fine root parameters were responsible for the majority of output

526 variance, whereas the phenology parameters contributed more than 20% of the variance for
 527 QVEGT and TLAI. In particular, the base temperature for the autumn phenology parameter
 528 (*phen_tbfall*) was sensitive, indicating the importance of quantifying the temperature effects on
 529 senescence accurately. Higher base temperatures were associated with smaller values of all
 530 carbon and water variables, reflecting the control of that parameter over growing season length
 531 (higher base temperature means earlier senescence given the same meteorological conditions).



532

533 **Fig. 5. Sensitivity of major carbon and water variables to model parameters for *Larix***
 534 ***laricina* and the shrub layer.** The height of each bar represents the percentage of the uncertainty
 535 of the examined carbon and water variables caused by a particular parameter. We only show 12
 536 out of 44 parameters (represented by colors) that have sensitivity indices large than 1%. Within
 537 each stacked bar, if the sensitivity is greater than 5%, a + or - symbol is included to show
 538 whether positive perturbations of that parameter result in a positive or negative deviation on the
 539 QoI. GPP is gC/m²/year; NPP is gC/m²/year; QVEGT is mm/year; TOTVEGC is gC/m²; and
 540 TLAI is m²/m².

541

542 For the shrub layer, the responses were found to be dominated by the shrub flnr (*flnr_Shruh*), the
 543 shrub stem to leaf allocation ratio (*stem_leaf_Shruh*), the shrub fine root to leaf allocation

544 (*froot_leaf_Shrub*), the shrub Ball-Berry stomatal conductance slope term (*mbbopt_Shrub*), and
545 the *phen_tbfall* and *phen_c* parameters. Perhaps unsurprisingly, parameters associated with the
546 *Picea* and *Sphagnum* were not identified as sensitive for the carbon and water variables of
547 deciduous conifer and shrub, indicating that belowground competition for water and nutrients in
548 the ELM among PFTs was not strongly affecting these QoIs. Overall, the two phenology
549 parameters (*phen_tbfall* and *phen_c*) contributed about 10% of the QoI variance. For both PFTs,
550 the high sensitivity of the *phen_c* parameter indicates the importance of representing and
551 accurately parameterizing chilling processes in the phenology sub-model.

552 **4 Discussion**

553 With the improved phenology processes incorporated, ELM_New demonstrated several
554 advantages over ELM_Default. ELM_Default without a chilling process showed little response
555 of spring onset to warming, whereas ELM_New with a chilling process showed strong
556 temperature sensitivity, which better matched the observations. This might be different from the
557 common understanding that a chilling requirement mediates the temperature sensitivity of spring
558 phenology (Chuine et al., 2016) because the spring onset simulated by ELM_Default occurs
559 when the accumulated temperature reaches a threshold, which is determined by the annual
560 average temperature in the previous year (Eq. 2). Such an algorithm was originally developed to
561 consider spatial heterogeneity of thermal requirement but may lead to a higher threshold of
562 thermal requirement at warmer enclosures in this study. Consequently, even though growing-
563 degree-day accumulated faster at warmer enclosures, the net result was a similar spring onset
564 across different temperature treatments; this was also discussed in Chen et al. (2016) from a
565 temporal perspective of climate warming. In contrast, the earlier spring onset in warmer

566 enclosures was better reproduced by ELM_New because of the improved mechanistic processes
567 represented by the accumulation of both winter chilling and spring thermal forcing (Eqs. 3–7).

568 In terms of the autumn senescence, ELM_Default is solely based on a daylength threshold,
569 which is partially supported by much evidence that photoperiod is the dominant cue for growth
570 cessation in temperate and boreal trees (Keller et al., 2011; Way and Montgomery, 2015).

571 However, such simplification could cause obvious biases in simulations of phenology and
572 phenological response to warming (Delpierre et al., 2009), requiring more realistic and process-
573 based improvement. In this study, ELM_New brought ELM_Default one step further toward this
574 improvement by considering the temperature regulation for autumn senescence. Such
575 temperature control was shown to be important at SPRUCE across different treatment levels
576 (Fig. 1) and was also confirmed by recent studies indicating that warming could significantly
577 delay the autumn senescence (Heide, 2011; Richardson et al., 2018b). Overall, ELM_New
578 showed earlier spring onset across all warming levels and earlier autumn senescence only at
579 lower warming levels but later autumn senescence at higher warming levels compared with
580 ELM_Default. Such changes caused by phenological model selection may have divergent effects
581 on carbon and water cycles at different warming levels as shown by this study (e.g., Figs. 2 and
582 S4) and previous ones (e.g., Kim et al., 2018; Piao et al., 2019b).

583 Our modeling results demonstrated significant phenological impacts on multiple processes
584 within the ELM. The most direct and considerable phenological effects identified to occur were
585 for LAI in terms of the seasonality and magnitude during the growing season. Such altered LAI
586 further induced a series of changes in the ELM vegetation-soil system, including enhanced
587 photosynthesis and water fluxes (Figs. 2 and S4), largely consistent with observational responses
588 of carbon and water cycles to phenology across different scales (Piao et al., 2007; Zeng et al.,

589 2017). Because the rate of soil carbon decomposition increases concurrently with warming, such
590 increased vegetation activities may not necessarily lead to a strengthened net land carbon sink
591 (Piao et al., 2019b). In this study, for example, the increase in ecosystem respiration exceeded
592 that of photosynthetic carbon gain and caused the NEP decrease in both winter and summer
593 seasons for the hummock (Fig. 4). In agreement with previous empirical findings (Kim et al.,
594 2018; Lian et al., 2020; Zeng et al., 2018), our results also showed notable influences of plant
595 phenological shifts on the water cycle, such as increased ET, lower soil moisture, and modified
596 runoff and ZWT during the growing season, especially under the eCO₂ conditions (Fig. 4).
597 Compared with ELM_Default, ELM_New produced enhanced photosynthesis, increased ET, and
598 lower soil moisture for plants only at higher warming levels, but such effects reversed at lower
599 warming levels because of earlier autumn senescence. At the grid-cell level, simulated carbon
600 and water fluxes were mainly affected by the two modified PFTs (*Larix laricina* and the shrub
601 layer), but also by the other two unmodified ones, *Picea mariana* and *Sphagnum*. Within an
602 ELM grid-cell, different PFTs receive identical environmental forcings and share the same soil
603 conditions. Therefore, the modifications in phenology of *Larix laricina* and the shrub layer could
604 alter the belowground soil characteristics, which further induced the carbon and water flux
605 changes of *Picea mariana* and *Sphagnum* (results not shown). When applying ELM_New onto
606 the studies of land-atmosphere feedbacks under future climate change, the phenological
607 influences by other environmental factors ought to be considered. For example, if droughts
608 become more pervasive or less water is available in late summer, the growing season length may
609 be reduced (because of earlier leaf senescence) instead of being lengthened, likely leading to a
610 decline in growing-season carbon fixation and ET (Lian et al., 2020).

611 The ELM phenology scheme will continue to be developed, including representation of
612 phenology responses to extreme events such as spring frost and droughts and optimization of
613 more phenological parameters over various vegetation types. For example, the unusually warm
614 March followed by severe spring frost in the extreme cold April in 2016 at SPRUCE caused
615 earlier spring onset and severe tissue mortality of *Larix laricina* in the warmest enclosures
616 (Richardson et al., 2018b). Such processes are completely lacking but urgently needed in most
617 land surface models, including the ELM, and are increasingly critical as extreme events become
618 more frequent and intense. Proper simulation of the impacts from extreme events on phenology
619 changes could be achieved by, for example, adding additional physiological limitations (e.g.,
620 hydraulic dynamics, freezing tolerance, impacts on foliar morphology) to current phenological
621 algorithms (Jensen et al. 2020). Moreover, the evergreen phenology scheme in the ELM, which
622 is currently active during the whole year, needs to be updated in the future. A recent study
623 revealed clear seasonal changes in the color and photosynthetic activity of evergreen conifer
624 forest using the PhenoCam observation of *Picea mariana* (Seyednasrollah et al., 2020). Based on
625 these new findings, adding spring and autumn phenological transitions to a certain percentage of
626 evergreen conifer canopy could improve the ELM evergreen phenology scheme.

627 ELM_New and associated site-level parameters could be upscaled onto broad scales through
628 linking the SPRUCE observations with other observational data sets and satellite images.

629 Regional phenological data from observational networks, such as the Pan European Phenology
630 Observation and USA National Phenology Network, could be examined in the future to verify
631 ELM_New and improve its capability in simulating phenology across various climate and
632 vegetation zones (Meng et al., 2021). Different upscaling strategies and methods, such as
633 merging local phenology observations with high-resolution satellite products (e.g., NASA's

634 MSLSP30NA Land Surface Phenology product derived from Harmonized Landsat Sentinel-2
635 data), may provide new insight into the modeling of large-scale phenology responses to a
636 changing climate (Pope et al., 2013; Bolton et al., 2020). Caution should be taken for the
637 upscaling process, especially for the SPRUCE shrub types. The mixed shrub layer at SPRUCE
638 mainly includes *Rhododendron groenlandicum* (Oeder) Kron and Judd (Labrador tea) and
639 *Chamaedaphne calyculata* (L.) Moench. (leatherleaf); the latter (occurring in cool temperate and
640 subarctic regions from North America to Finland and Japan) is more representative than the
641 former (occurring only in North America) for the shrubs in northern high latitudes. However,
642 current PhenoCam signals for deciduous shrubs are merely a mix of these two types, thus
643 limiting the clean upscaling for individual shrub species.

644 Sensitivity analysis in this study showed that parameter uncertainty of the phenology model
645 significantly drove the prediction uncertainty of carbon and water cycles; this suggests that
646 further regional-scale observations across vegetation types and model developments remain
647 necessary to reduce uncertainties regarding chilling effects on spring phenology and autumn
648 temperature constraints on fall senescence. The extending time series of phenology and
649 environment observations at SPRUCE that cover a wider range of conditions over time will be
650 helpful to further reduce the model uncertainties. Future model evaluation and development
651 processes may be also guided by more comprehensive uncertainty quantification studies,
652 including examining the sensitivities of simulated carbon, water, and nutrient cycling to
653 phenological responses under extreme events, such as spring frosts and freezes, droughts, and
654 wildfires.

655 **5 Conclusions**

656 Using the latest experimental observations from SPRUCE, this study evaluated and improved
657 seasonal-deciduous phenology components of ELM and investigated possible phenological
658 feedbacks to major carbon and water fluxes. Selected mechanism-based phenology models of
659 spring onset and autumn senescence were introduced, in which the timing of spring onset
660 depends on both winter chilling and spring thermal forcing processes, whereas the timing of
661 autumn senescence relies on the co-limitation of daylength and temperature. In contrast to the
662 default ELM, the revised model better captured the PhenoCam observations (i.e., distinct
663 seasonal phenology of *Larix laricina* and the shrub layer and linearly extended growing season
664 length in response to warming). In addition, the improved ELM produced intensified carbon and
665 water fluxes associated with a longer growing season and stronger temperature response of
666 vegetation, especially under eCO₂ and warmer conditions. A model sensitivity analysis further
667 indicated that phenology parameters contributed significantly to simulated carbon and water
668 cycle variations over interannual timescales. This practice of model-experimental coupling
669 highlights the importance of phenological processes in affecting complex terrestrial-climate
670 interactions, and it facilitates the uncertainty reduction of E3SM in predicting Earth dynamics at
671 broad spatiotemporal scales.

672 **Acknowledgments, Samples, and Data**

673 This work was supported by the Terrestrial Ecosystem Science Scientific Focus Area project
674 funded by the US Department of Energy, Office of Science, Office of Biological and
675 Environmental Research. Oak Ridge National Laboratory is supported by the Office of Science
676 of the US Department of Energy under Contract No. DE-AC05-00OR22725. This research used
677 resources of the Compute and Data Environment for Science (CADES) at Oak Ridge National
678 Laboratory. L. Meng is also supported by NASA FINESST Program (80NSSC19K1356). ADR
679 acknowledges support from the NSF (DEB 1702697).

680 **Data and materials availability:** PhenoCam datasets and environmental measurements
681 pertaining to this study are in the online project archive at <http://mnspruce.ornl.gov> and for long-
682 term storage in the US Department of Energy's Environmental Systems Science Data
683 Infrastructure for a Virtual Ecosystem (ESS-DIVE; <http://ess-dive.lbl.gov/>).

684 **References**

- 685 Bolton, D.K. et al., 2020. Continental-scale land surface phenology from harmonized Landsat 8 and Sentinel-2
686 imagery. *Remote Sensing of Environment*, 240, 111685.
- 687 Caffarra, A., Donnelly, A. and Chuine, I., 2011. Modelling the timing of *Betula pubescens* budburst. II. Integrating
688 complex effects of photoperiod into process-based models. *Climate Research*, 46(2): 159–170.
- 689 Cannell, M. and Smith, R., 1983. Thermal time, chill days and prediction of budburst in *Picea sitchensis*. *Journal of*
690 *applied Ecology*: 951–963.
- 691 Cesaraccio, C., Spano, D., Snyder, R.L. and Duce, P., 2004. Chilling and forcing model to predict bud-burst of crop
692 and forest species. *Agricultural and Forest Meteorology*, 126(1–2): 1–13.
- 693 Chen, M., Melaas, E.K., Gray, J.M., Friedl, M.A. and Richardson, A.D., 2016. A new seasonal-deciduous spring
694 phenology submodel in the Community Land Model 4.5: impacts on carbon and water cycling under future
695 climate scenarios. *Global Change Biology*, 22(11): 3675–3688.
- 696 Chuine, I. and Régnière, J., 2017. Process-Based Models of Phenology for Plants and Animals. *Annual Review of*
697 *Ecology, Evolution, and Systematics*, 48(1): 159–182.
- 698 Chuine, I. et al., 2016. Can phenological models predict tree phenology accurately in the future? The unrevealed
699 hurdle of endodormancy break. *Global Change Biology*, 22(10): 3444–3460.
- 700 Cremonese, E. et al. 2017. Heat wave hinders green wave: The impact of climate extreme on the phenology of a
701 mountain grassland. *Agricultural and Forest Meteorology* 247: 320–330.
- 702 Dahlin, K., Fisher, R. and Lawrence, P., 2015. Environmental drivers of drought deciduous phenology in the
703 Community Land Model. *Biogeosciences*, 12(16): 5061–5074.
- 704 Debusschere, N., Segers, P., Dubruel, P., Verhegghe, B. and De Beule, M., 2015. A finite element strategy to
705 investigate the free expansion behaviour of a biodegradable polymeric stent. *Journal of Biomechanics*,
706 48(10): 2012–2018.
- 707 Delpierre, N. et al., 2009. Modelling interannual and spatial variability of leaf senescence for three deciduous tree
708 species in France. *agricultural and forest meteorology*, 149(6–7): 938–948.
- 709 Dufrêne, E. et al., 2005. Modelling carbon and water cycles in a beech forest: Part I: Model description and
710 uncertainty analysis on modelled NEE. *Ecological Modelling*, 185(2–4): 407–436.
- 711 Forsythe, W.C., Rykiel Jr, E.J., Stahl, R.S., Wu, H.-i. and Schoolfield, R.M., 1995. A model comparison for
712 daylength as a function of latitude and day of year. *Ecological Modelling*, 80(1): 87–95.
- 713 Fracheboud, Y. et al., 2009. The control of autumn senescence in European aspen. *Plant physiology*, 149(4): 1982–
714 1991.
- 715 Hannerz, M., Ekberg, I. and Norell, L., 2003. Variation in chilling requirements for completing bud rest between
716 provenances of Norway spruce. *Silvae Genetica*, 52(3–4): 161–168.

- 717 Hänninen, H. et al., 2019. Experiments Are Necessary in Process-Based Tree Phenology Modelling. *Trends in Plant*
718 *Science*, 24(3): 199–209.
- 719 Hanson, P.J. et al., 2017. Attaining whole-ecosystem warming using air and deep-soil heating methods with an
720 elevated CO₂ atmosphere. *Biogeosciences (Online)*, 14(4): 861–883.
- 721 Hanson, P.J. et al., 2020. Rapid net carbon loss from a whole-ecosystem warmed Peatland. *AGU Advances*, 1(3):
722 e2020AV000163.
- 723 Heide, O.M., 2011. Temperature rather than photoperiod controls growth cessation and dormancy in *Sorbus* species.
724 *Journal of experimental botany*, 62(15): 5397–5404.
- 725 Jeong, S.J. and Medvigy, D., 2014. Macroscale prediction of autumn leaf coloration throughout the continental U
726 nited States. *Global Ecology and Biogeography*, 23(11): 1245–1254.
- 727 Keenan, T.F. and Richardson, A.D., 2015. The timing of autumn senescence is affected by the timing of spring
728 phenology: implications for predictive models. *Global change biology*, 21(7): 2634–2641.
- 729 Keller, S.R. et al., 2011. Climate-driven local adaptation of ecophysiology and phenology in balsam poplar, *Populus*
730 *balsamifera* L.(Salicaceae). *American Journal of Botany*, 98(1): 99–108.
- 731 Keskitalo, J., Bergquist, G., Gardeström, P. and Jansson, S., 2005. A cellular timetable of autumn senescence. *Plant*
732 *Physiology*, 139(4): 1635–1648.
- 733 Kim, J.H. et al., 2018. Warming-induced earlier greenup leads to reduced stream discharge in a temperate mixed
734 forest catchment. *Journal of Geophysical Research: Biogeosciences*, 123(6): 1960–1975.
- 735 Kolka, R., Sebestyen, S., Verry, E.S. and Brooks, K., 2011. Peatland biogeochemistry and watershed hydrology at
736 the Marcell Experimental Forest. CRC Press.
- 737 Körner, C. and Basler, D., 2010a. Phenology under global warming. *Science*, 327(5972): 1461–1462.
- 738 Körner, C. and Basler, D., 2010b. Response—Warming, Photoperiods, and Tree Phenology. *Science*, 329(5989):
739 278–278.
- 740 Landsberg, J., 1974. Apple fruit bud development and growth; analysis and an empirical model. *Annals of Botany*,
741 38(5): 1013–1023.
- 742 Lawrence, D.M. et al., 2011. Parameterization improvements and functional and structural advances in version 4 of
743 the Community Land Model. *Journal of Advances in Modeling Earth Systems*, 3(1): M03001.
- 744 Li, H., et al. 2016. Evapotranspiration dynamics over a temperate meadow ecosystem in eastern Inner Mongolia,
745 China. *Environmental Earth Sciences*, 75(11): 978.
- 746 Lian, X. et al., 2020. Summer soil drying exacerbated by earlier spring greening of northern vegetation. *Science*
747 *advances*, 6(1): eaax0255.
- 748 Liang, L., 2019. A spatially explicit modeling analysis of adaptive variation in temperate tree phenology.
749 *Agricultural and Forest Meteorology*, 266: 73–86.

750 Liu, Q. et al., 2020. Modeling leaf senescence of deciduous tree species in Europe. *Global Change Biology*, 26(7):
751 4104–4118.

752 Liu, Z. et al. 2015. Relationship between leaf physiologic traits and canopy color indices during the leaf expansion
753 period in an oak forest. *Ecosphere* 6(12): 1–9.

754 Meng, L. et al. 2021. Photoperiod decelerates the advance of spring phenology of six deciduous tree species under
755 climate warming. *Global Change Biology*.

756 Meng, L. et al., 2020a. Urban warming advances spring phenology but reduces the response of phenology to
757 temperature in the conterminous United States. *Proceedings of the National Academy of Sciences*, 117(8):
758 4228–4233.

759 Meng, L. et al., 2020b. Divergent responses of spring phenology to daytime and nighttime warming. *Agricultural
760 and Forest Meteorology*, 281: 107832.

761 Menzel, A. and Fabian, P., 1999. Growing season extended in Europe. *Nature*, 397(6721): 659–659.

762 Migliavacca, M. et al., 2008. European larch phenology in the Alps: can we grasp the role of ecological factors by
763 combining field observations and inverse modelling? *International journal of biometeorology*, 52(7): 587–
764 605.

765 Murray, M., Cannell, M. and Smith, R., 1989. Date of budburst of fifteen tree species in Britain following climatic
766 warming. *Journal of Applied Ecology*, 26(2): 693–700.

767 Oleson, K., 2013. Technical description of version 4.5 of the Community Land Model (CLM), Natl. Cent. for
768 Atmos. Res., Tech. Note NCAR/TN-503+ STR.

769 Peano, D. et al., 2020. Plant phenology evaluation of CRESCENDO land surface models–Part I: Start and end of
770 growing season. *Biogeosciences*, 18: 2405–2428.

771 Peichl, M. 2015. Bringing color into the picture: using digital repeat photography to investigate phenology controls
772 of the carbon dioxide exchange in a boreal mire. *Ecosystems*, 18.1: 115–131.

773 Piao, S. et al., 2019a. Plant phenology and global climate change: Current progresses and challenges. *Global change
774 biology*, 25(6): 1922–1940.

775 Piao, S. et al., 2019b. Characteristics, drivers and feedbacks of global greening. *Nature Reviews Earth &
776 Environment*, 1: 14–27.

777 Piao, S., Friedlingstein, P., Ciais, P., Viovy, N. and Demarty, J., 2007. Growing season extension and its impact on
778 terrestrial carbon cycle in the Northern Hemisphere over the past 2 decades. *Global Biogeochemical
779 Cycles*, 21(3): GB3018.

780 Pope, K.S. et al., 2013. Detecting nonlinear response of spring phenology to climate change by Bayesian analysis.
781 *Global Change Biology*, 19(5): 1518–1525.

782 Reaumur, R.d., 1735. Observations du thermomètre faites à Paris pendant l'année 1735, comparées avec celles qui
783 ont été faites sous la ligne, à l'Isle de France, à Alger et quelques unes de nos îles de l'Amérique. Mémoires
784 l'Académie R des Sci: 545–576.

785 Ricciuto, D., Sargsyan, K. and Thornton, P., 2018. The impact of parametric uncertainties on biogeochemistry in the
786 E3SM land model. *Journal of Advances in Modeling Earth Systems*, 10(2): 297–319.

787 Ricciuto, D., X. Xu, X. Shi, Y. Wang, X. Song, C.W. Schadt, N.A. Griffiths, J. Mao, J.M. Warren, P.E. Thornton, J.
788 Chanton, J.K. Keller, S. Bridgham, J. Gutknecht, S.D. Sebestyen, A. Finzi, R. Kolka, P.J. Hanson, 2020.
789 An integrative model for soil biogeochemistry and methane processes: I. model structure and sensitivity
790 analysis, Accepted, *Journal of Geophysical Research-Biogeosciences*.

791 Richardson, A.D. et al., 2007. Use of digital webcam images to track spring green-up in a deciduous broadleaf
792 forest. *Oecologia*, 152(2): 323–334.

793 Richardson, A.D. et al., 2012. Terrestrial biosphere models need better representation of vegetation phenology:
794 results from the North American Carbon Program Site Synthesis. *Global Change Biology*, 18(2): 566–
795 584.

796 Richardson, A.D. et al., 2013. Climate change, phenology, and phenological control of vegetation feedbacks to the
797 climate system. *Agricultural and Forest Meteorology*, 169: 156–173.

798 Richardson, A.D. et al., 2018a. Tracking vegetation phenology across diverse North American biomes using
799 PhenoCam imagery. *Scientific Data*, 5: 180028.

800 Richardson, A.D. et al., 2018b. Ecosystem warming extends vegetation activity but heightens vulnerability to cold
801 temperatures. *Nature*, 560: 368–371.

802 Sargsyan, K. et al., 2014. Dimensionality reduction for complex models via Bayesian compressive sensing.
803 *International Journal for Uncertainty Quantification*, 4(1): 63–93.

804 Sarvas, R., 1972. Investigations on the annual cycle of development of forest trees. Active period. Investigations on
805 the annual cycle of development of forest trees. Active period. *Metsantutkimuslaitoksen Julkaisuja*, 76(3).

806 Sarvas, R., 1974. Investigations on the annual cycle of development of forest trees. Autumn dormancy and winter
807 dormancy. *Communicationes Linstitututi Forestalis Fenniae*, 84: 1–101.

808 Schädel, C. et al., 2019. SPRUCE Vegetation Phenology in Experimental Plots from Phenocam Imagery, 2015-
809 2018, Oak Ridge National Laboratory, Oak Ridge, TN (United States).

810 Schwartz, M.D., 1992. Phenology and springtime surface-layer change. *Monthly weather review*, 120(11): 2570–
811 2578.

812 Seyednasrollah, B. et al., 2019. Tracking vegetation phenology across diverse biomes using Version 2.0 of the
813 PhenoCam Dataset. *Scientific Data*, 6(1): 222.

814 Seyednasrollah, B. et al., 2020. Seasonal variation in the canopy color of temperate evergreen conifer forests. *New
815 Phytologist*, 229: 2586–2600.

816 Shi, X. et al., 2015. Representing northern peatland microtopography and hydrology within the Community Land
817 Model. *Biogeosciences Discussions (Online)*, 12(4).

818 Shi, X. et al., 2020. Modeling the hydrology and physiology of Sphagnum moss in a northern temperate bog.
819 *Biogeosciences Discussions*: 1–49.

820 Sonnentag, O. et al., 2012. Digital repeat photography for phenological research in forest ecosystems. *Agricultural
821 and Forest Meteorology*, 152: 159–177.

822 Thornton, P.E. et al., 2002. Modeling and measuring the effects of disturbance history and climate on carbon and
823 water budgets in evergreen needleleaf forests. *Agricultural and forest meteorology*, 113(1–4): 185–222.

824 Wang, K. et al., 2013. Evaluation of CLM4 solar radiation partitioning scheme using remote sensing and site level
825 FPAR datasets. *Remote Sensing*, 5(6): 2857–2882.

826 Way, D.A. and Montgomery, R.A., 2015. Photoperiod constraints on tree phenology, performance and migration in
827 a warming world. *Plant, Cell & Environment*, 38(9): 1725–1736.

828 White, M.A. et al., 2009. Intercomparison, interpretation, and assessment of spring phenology in North America
829 estimated from remote sensing for 1982–2006. *Global Change Biology*, 15(10): 2335–2359.

830 White, M.A., Thornton, P.E. and Running, S.W., 1997. A continental phenology model for monitoring vegetation
831 responses to interannual climatic variability. *Global biogeochemical cycles*, 11(2): 217–234.

832 Zeng, Z. et al., 2017. Climate mitigation from vegetation biophysical feedbacks during the past three decades.
833 *Nature Climate Change*, 7(6): 432–436.

834 Zeng, Z. et al., 2018. Impact of Earth greening on the terrestrial water cycle. *Journal of Climate*, 31(7): 2633–2650.

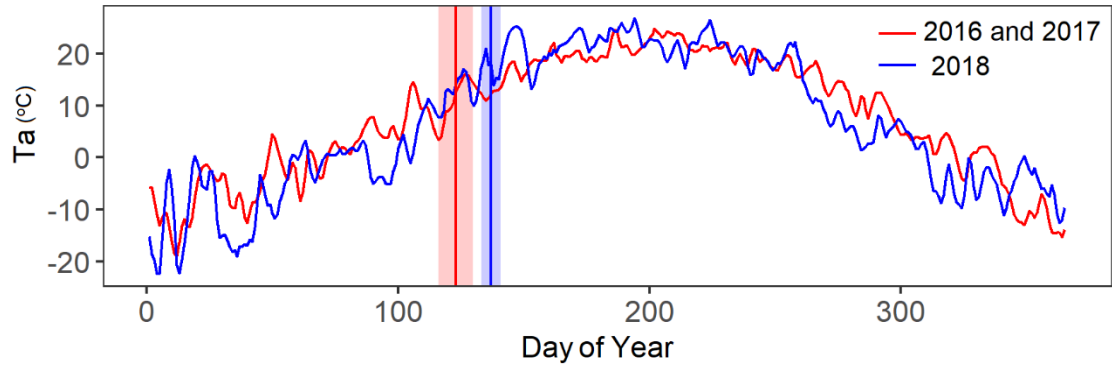
835

836
837
838
839
840
841
842
843
844
845
846
847
848
849
850
851
852
853
854
855

Supplementary Material for

**Evaluation and Modification of ELM Seasonal Deciduous Phenology against
Observations in a Southern Boreal Peatland Forest**

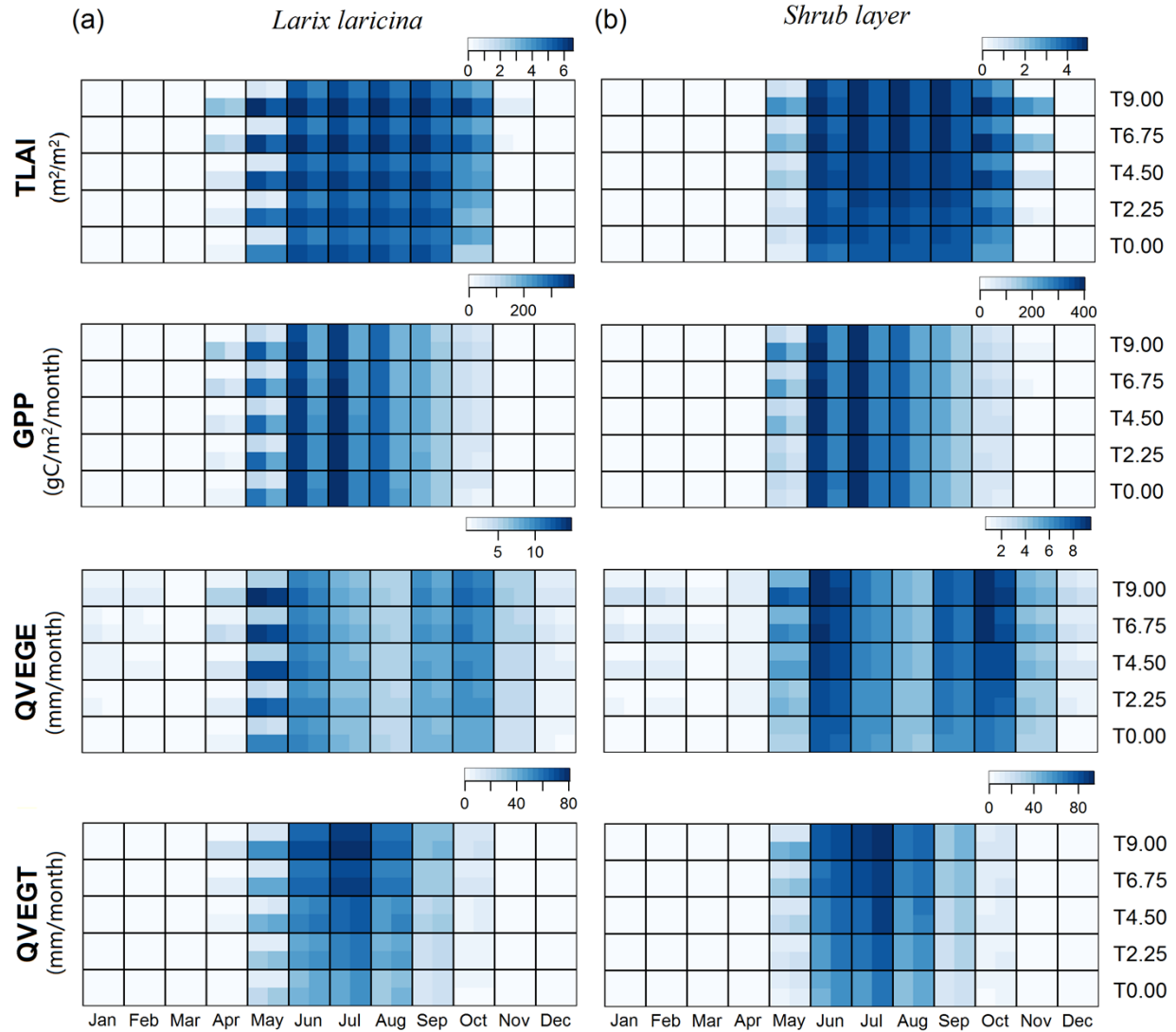
This PDF contains:
Figures S1–S9
Tables S1–S3



856

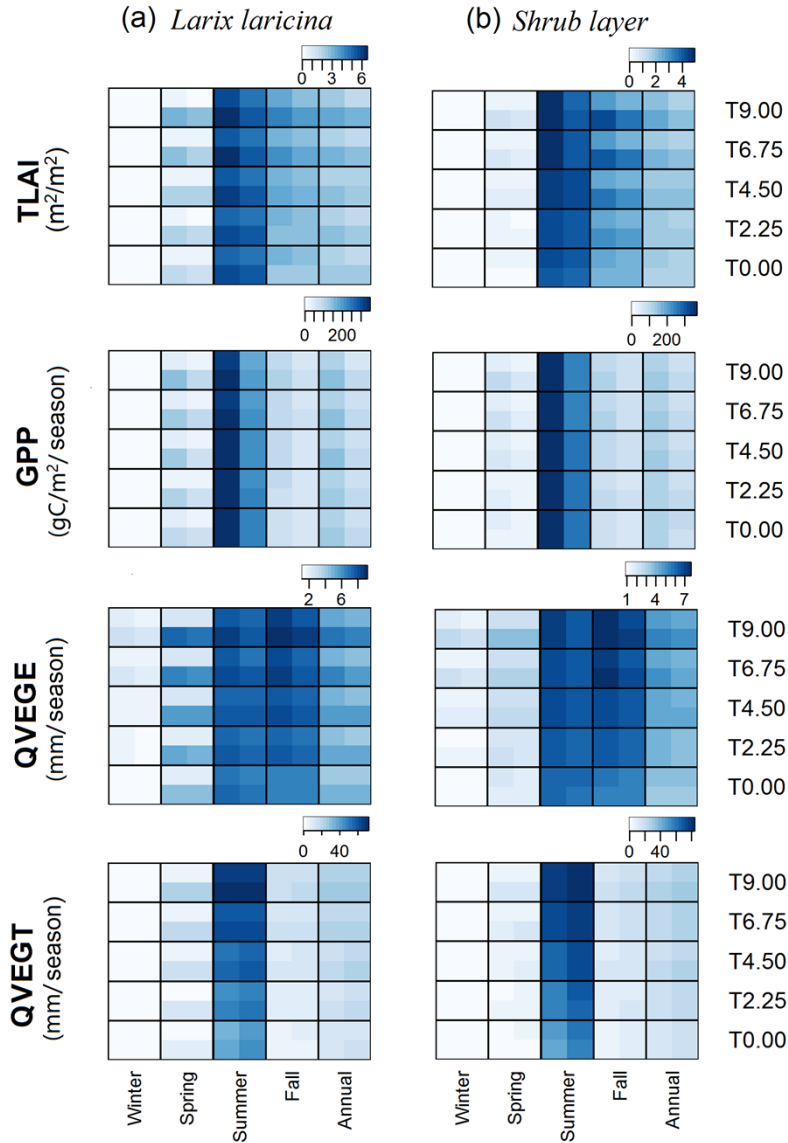
857 **Fig. S1. 2 m air temperature and spring onset dates in 2018 in comparison to in 2016 and**
 858 **2017.** Air temperature shown here is 3-day averaged temperature at 2 m on central tower at plot
 859 06 (0 °C warming and aCO₂), spatially averaged from two replicates. Red line represents mean
 860 air temperature during 2016 and 2017. Blue line represents air temperature during 2018. Vertical
 861 lines and shadow represent the mean and standard deviation of spring onset dates across all
 862 enclosures, respectively.

863



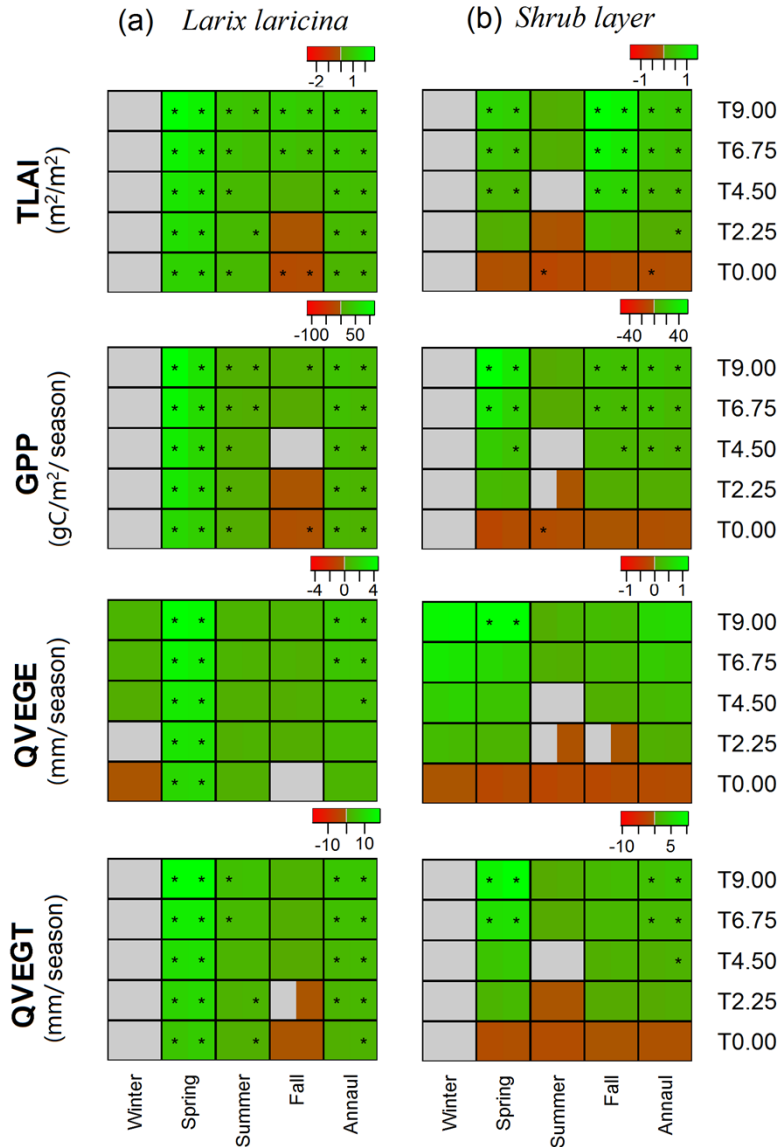
864

865 **Fig. S2. Predicted monthly TLAI, GPP, QVEGE, and QVEGT by ELM_Default and**
 866 **ELM_New for *Larix laricina* (a) and the shrub layer (b).** The value is the inter-annual mean
 867 during 2016 to 2018. Four pixels are within each grid. The left and right columns represent value
 868 at eCO₂ and aCO₂ chambers, respectively, and the top and bottom rows represent values
 869 predicted by ELM_Default and ELM_New, respectively.



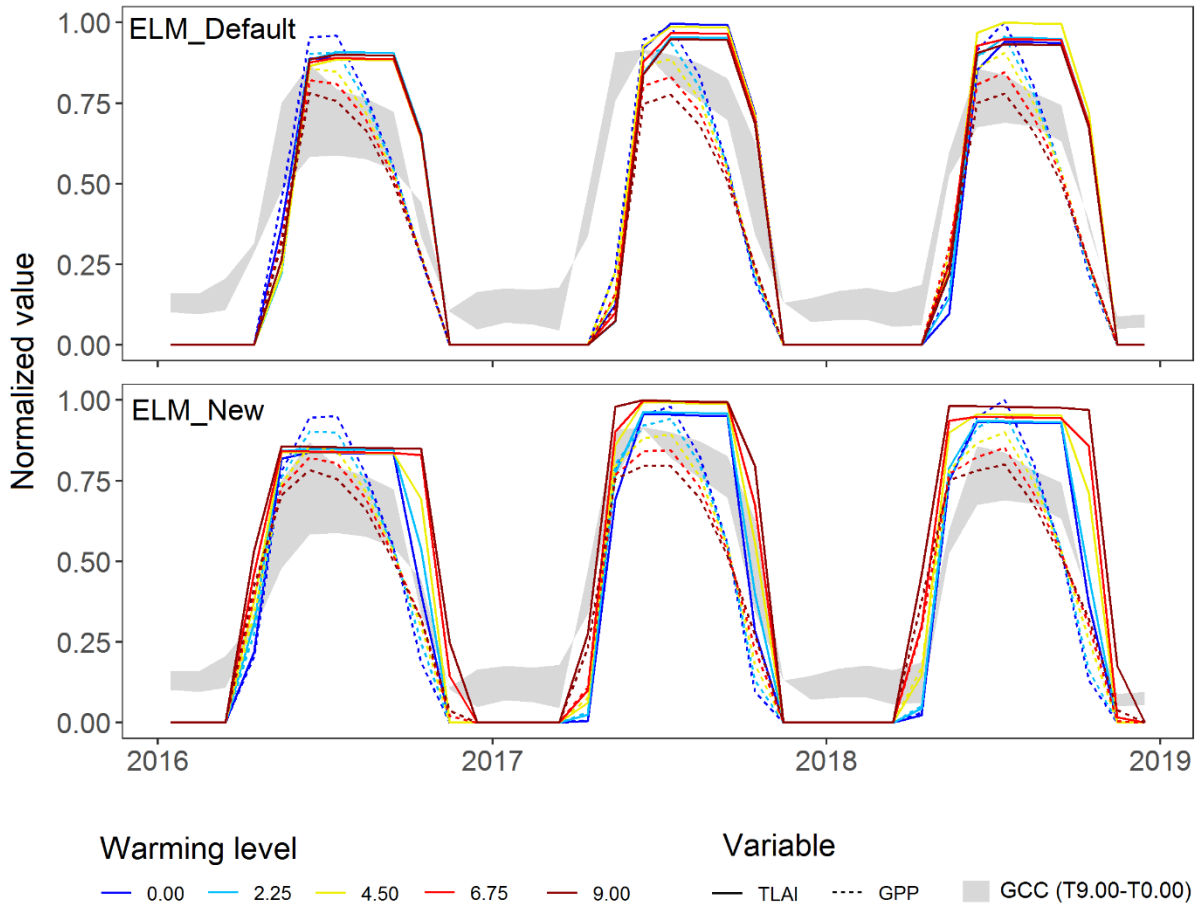
870

871 **Fig. S3. Predicted seasonal TLAI, GPP, QVEGE, and QVEGT by ELM_Default and**
 872 **ELM_New for *Larix laricina* (a) and the shrub layer (b).** The value is the inter-annual mean
 873 during 2016 to 2018. Four pixels are within each grid. The left and right columns represent value
 874 at eCO₂ and aCO₂ chambers, respectively, and the top and bottom rows represent value predicted
 875 by ELM_Default and ELM_New, respectively.



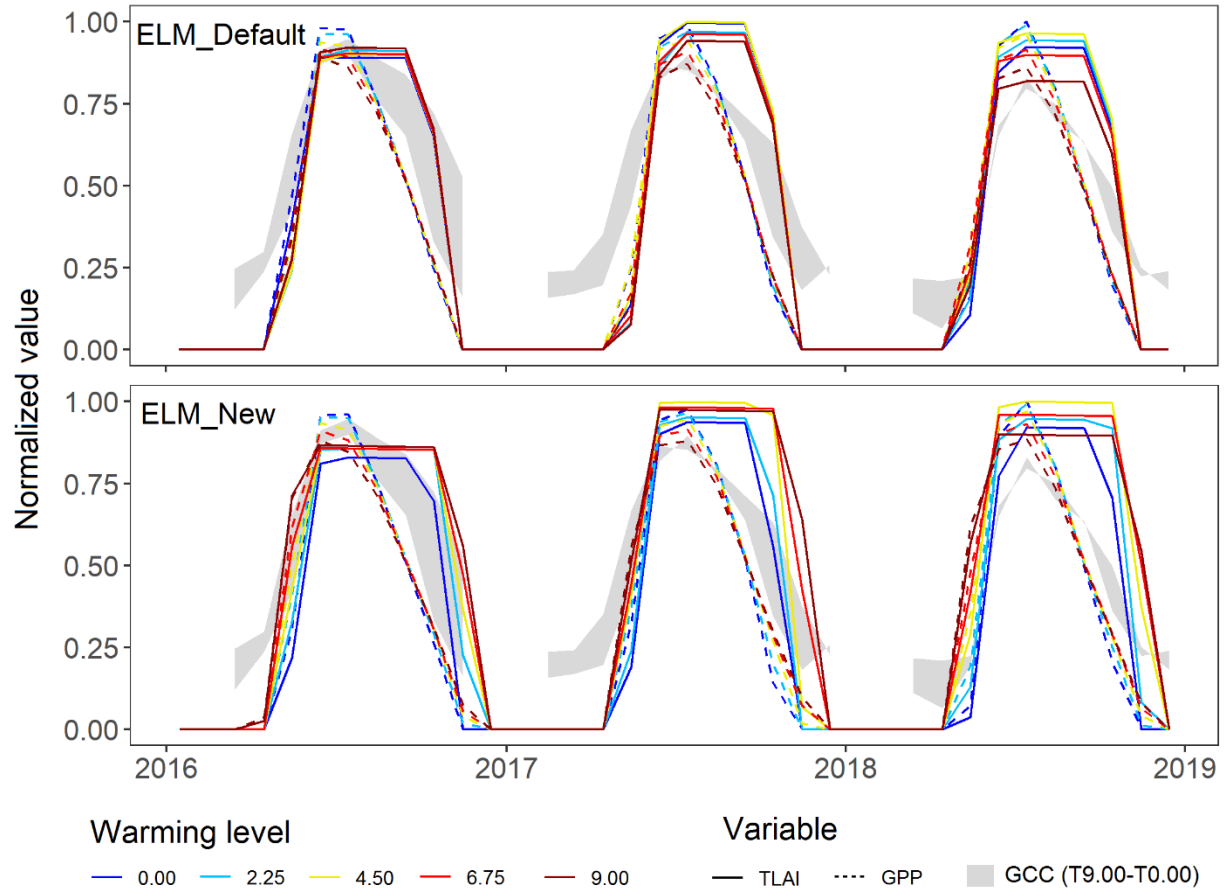
876

877 **Fig. S4. Changes in predicted seasonal TLAI, GPP, QVEGE, and QVEGT by**
 878 **ELM_Default and ELM_New for *Larix laricina* (a) and the shrub layer (b).** The value is the
 879 inter-annual mean during 2016 to 2018. Green represents higher values by ELM_New, brown
 880 represents lower values by ELM_New, and gray represents no differences between ELM_New
 881 and ELM_Default. Four pixels are within each grid. The left and right columns represent value at
 882 eCO₂ and aCO₂ chambers, respectively. Stars indicate significant differences between
 883 ELM_New and ELM_Default based on a two-tailed Student's *t* test ($P < 0.1$).



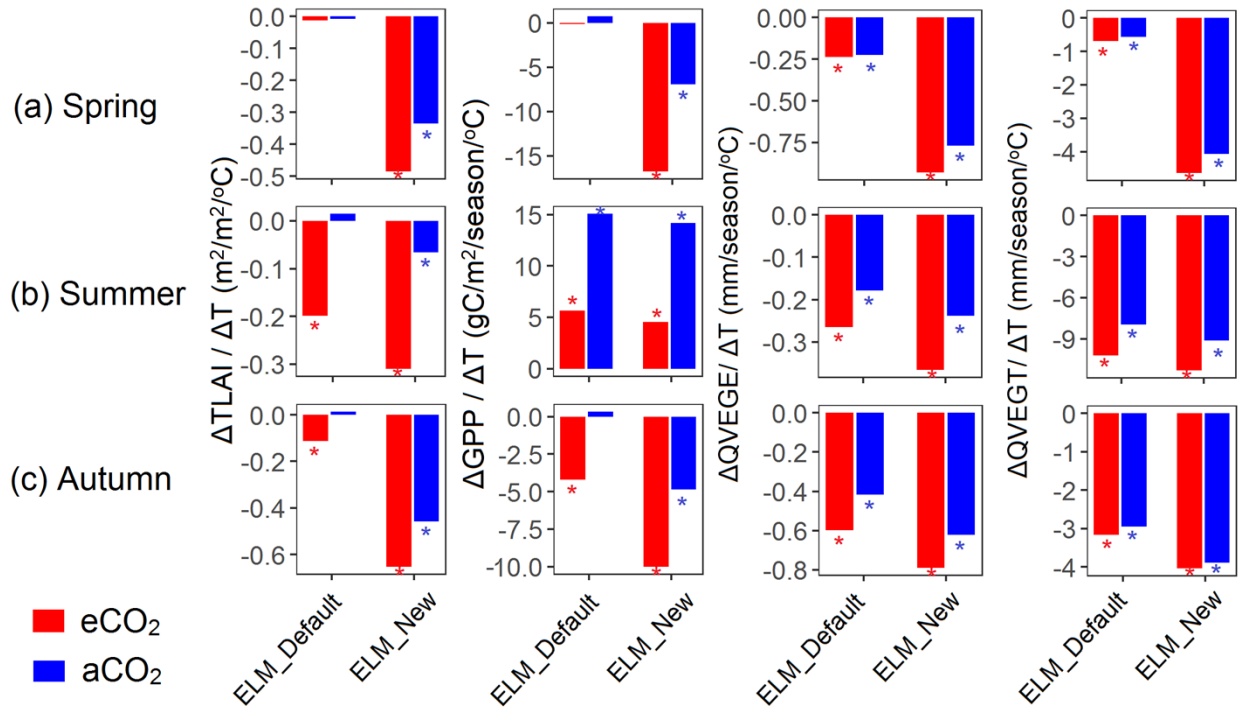
884

885 **Fig. S5. TLAI, GPP, and G_{CC} of *Larix laricina* during 2016 to 2018 at aCO₂ across five**
 886 **warming levels.** The y-axis is the normalized value of each variable. The shadow of G_{CC}
 887 represents the range of G_{CC} at 0°C and 9°C warming chambers. Normalization is conducted for
 888 each variable across all warming levels during 2016 to 2018, and separately for ELM_Default
 889 and ELM_New.



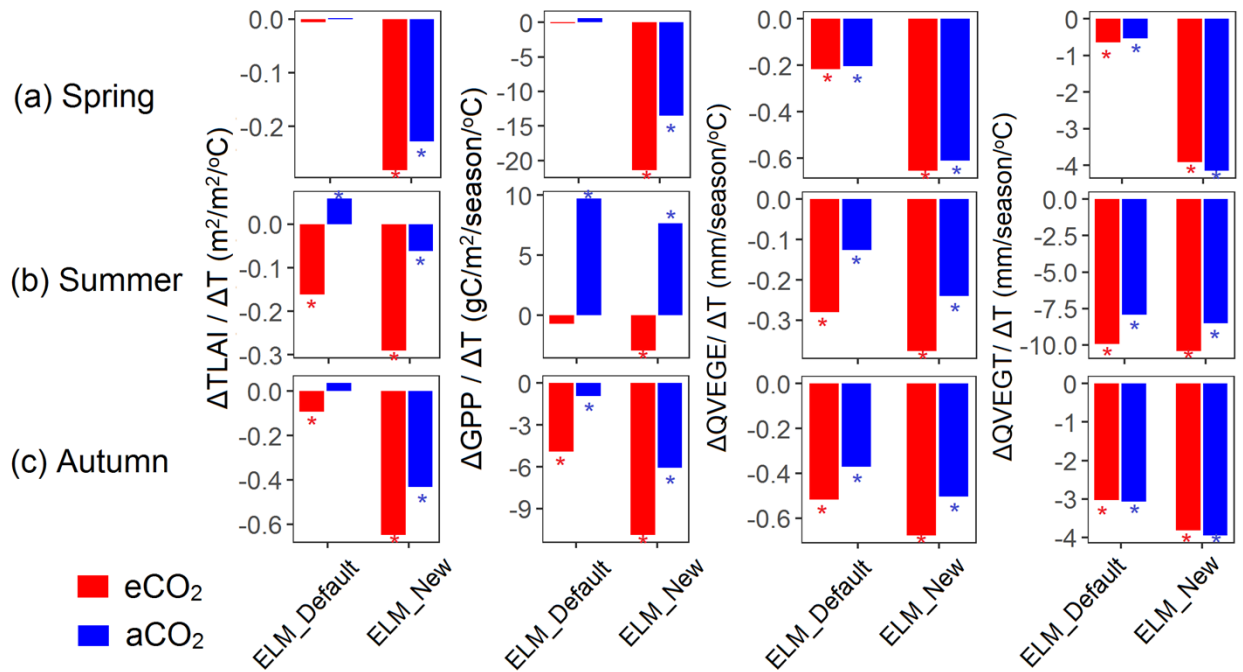
890

891 **Fig. S6. TLAI, GPP, and G_{CC} of the shrub layer during 2016 to 2018 at aCO_2 across five**
 892 **warming levels.** The y-axis is the normalized value of each variable. The shadow of G_{CC}
 893 represents the range of G_{CC} at $0^\circ C$ and $9^\circ C$ warming chambers. Normalization is conducted for
 894 each variable across all warming levels during 2016 to 2018, and separately for ELM_Default
 895 and ELM_New.



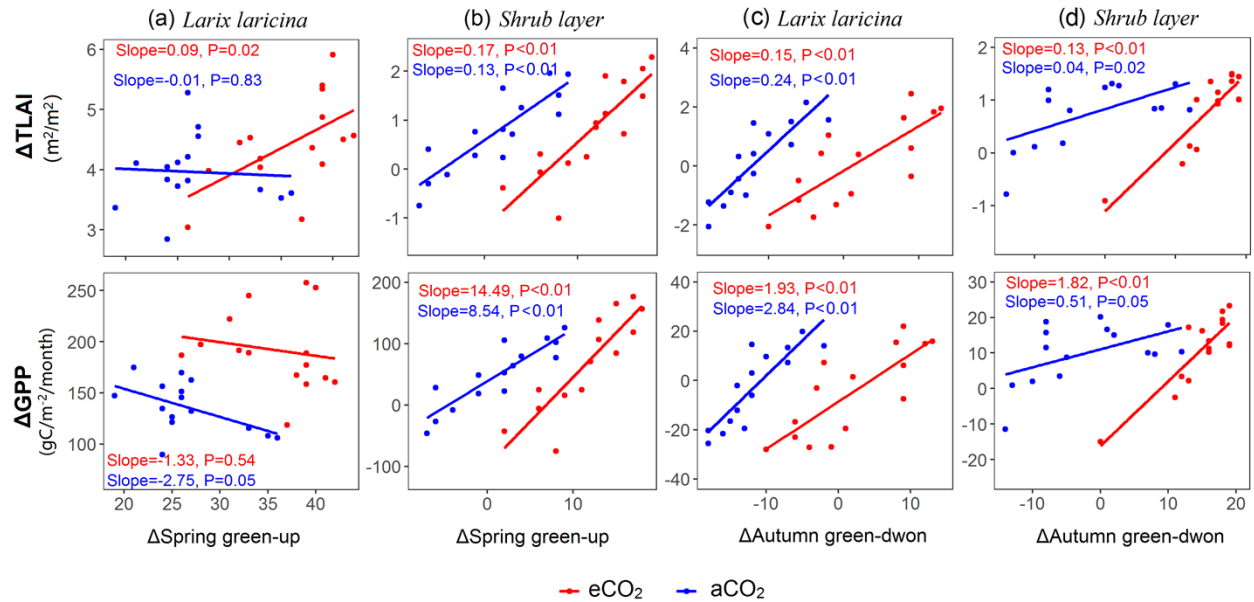
896

897 **Fig. S7. Temperature responses of carbon and water fluxes of *Larix laricina* to warming**
 898 **and elevated CO₂ predicted by ELM_Default and ELM_New for spring (a), summer (b),**
 899 **and autumn (c).** There is no value in winter. The temperature responses are calculated as the
 900 slope of linear regression between carbon/water variables and warming levels. Significance is
 901 shown ($P < 0.1$). TLAI is m^2/m^2 ; GPP is $gC/m^2/month$; QVEGE is $mm/month$; and QVEGT is
 902 $mm/month$.



903

904 **Fig. S8. Temperature responses of carbon and water fluxes of shrub layer to warming and**
 905 **elevated CO₂ predicted by ELM_Default and ELM_New for spring (a), summer (b), and**
 906 **autumn (c).** There is no value in winter. The temperature responses are calculated as the slope of
 907 linear regression between carbon/water variables and warming levels. Significance is shown
 908 ($P < 0.1$). TLAI is m²/m²; GPP is gC/m²/month; QVEGE is mm/month; and QVEGT is
 909 mm/month.



910

911 **Fig. S9. The relationship between differences in TLAI and GPP and differences in spring**
 912 **green-up (a, b) and autumn green-down (c, d) simulated by ELM_Default and ELM_New.**
 913 The linear regression lines, slopes, and *P* values are shown in each figure. The ΔTLAI, ΔGPP,
 914 and ΔAutumn green-down are calculated by subtracting ELM_Default from ELM_New. ΔSpring
 915 green-up is calculated by subtracting ELM_New from ELM_Default. a, b: ΔTLAI and ΔGPP are
 916 in May; c, d: ΔTLAI and ΔGPP are in October.

917 **Table S1. Statistics in model calibration.**

Vegetation type	Spring onset model				Autumn senescence model			Statistic		
	<i>a</i>	<i>b</i>	<i>c</i>	T_{base} (F)	$Pstart$ (s)	$Ycrit$	Tb (F)	LL	AIC	$AICc$
<i>Larix laricina</i>	9	2,112	-0.04	279.50	46,800	1,750	294.5	71.93	157.86	164.4
Shrub layer	33	1,388	-0.02	279.05	54,600	1,600	290.15	90.46	194.92	201.5

918 LL : log likelihood, AIC : Akaike information criterion

919 **Table S2. Statistics in model evaluation during 2018.** There is no correlation in autumn green-
 920 down between ELM_Default and PhenoCam observation, due to the unchanged in autumn
 921 green-down across warming levels by ELM_Default.

Model	Vegetation type	Spring onset model		Autumn senescence model	
		RMSE	Correlation	RMSE	Correlation
ELM_Default	<i>Larix laricina</i>	26.3	0.18	9.1	—
	Shrub layer	3.4	0.41	7.6	—
ELM_New	<i>Larix laricina</i>	8.2	0.34	11.9	-0.22
	Shrub layer	7.4	0.50	13.4	0.21

922

923 **Table S3. Parameters and ranges used in the GSA.**

Parameter	Description	Min	Max
flnr ¹	Rubisco-N fraction of leaf N	0.05	0.30
croot_stem ¹	Coarse root to stem allocation ratio	0.05	0.8
stem_leaf ¹	Stem to leaf allocation ratio	0.3	2.2
leaf_long ¹	Leaf longevity (yr)	0.75	2.0
slatop ¹	Specific leaf area at canopy top (m ² gC ⁻¹)	0.004	0.04
leafcn ¹	Leaf C to N ratio	20	75
froot_leaf ¹	Fine root to leaf allocation ratio	0.15	2.0
mp ¹	Ball-Berry stomatal conductance slope	4.5	12
r_mort	Vegetation mortality	0.005	0.1
decomp_depth_efolding	Depth-dependence e-folding depth for decomposition (m)	0.2	0.7
q _{drai,0}	Maximum subsurface drainage rate (kg m ⁻² s ⁻¹)	0	1e-3
Q _{10_mr}	Temperature sensitivity of maintenance respiration	1.2	3.0
br_mr	Base rate for maintenance respiration (gC gN m ² s ⁻¹)	1e-6	5e-6
crit_onset_gdd	Critical growing degree days for leaf onset	20	500
lw_top_ann	Live wood turnover proportion (yr ⁻¹)	0.2	0.85
gr_perc	Growth respiration fraction	0.12	0.4
r _{drai,0}	Coefficient for surface water runoff (kg m ⁻⁴ s ⁻¹)	1e-9	1e-6
phen_a	A parameter for spring onset process	1.0	30.0
phen_b	A parameter for spring onset process	1,000	2,500
phen_c	A parameter for spring onset process	-0.06	-0.01
phen_tbspring	Base temperature for spring onset process	269.15	282.15
phen_tbfall	Base temperature for autumn senescence process	272.15	308.15
phen_ycrit	Threshold to trigger autumn senescence	1,000	2,000
phen_pstart	Photoperiod threshold for autumn senescence process	12.0	16.5

924 ¹PFT-specific parameters